Progress in Polymer Science 105 (2020) 101242

Contents lists available at ScienceDirect

Progress in Polymer Science

journal homepage: www.elsevier.com/locate/ppolysci

Dynamics of polymer segments, polymer chains, and nanoparticles in polymer nanocomposite melts: A review

Eric J. Bailey*, Karen I. Winey*

Department of Materials Science and Engineering, University of Pennsylvania, Philadelphia, PA 19104, United States

ARTICLE INFO

Article history:
Available online 14 April 2020

Keywords:
Polymer nanocomposites
Segmental dynamics
Polymer diffusion
Nanoparticle diffusion
Glass transition

ABSTRACT

The addition of nanoparticles (NPs) to a polymer matrix, forming a polymer nanocomposite (PNC), is known to alter the microscopic dynamic processes of both species which leads to unique macroscopic material properties of the PNC. Because the NPs and polymers have overlapping characteristic length, time, and energy scales, the interactions within these materials are complex and the dynamics are interrelated. In this review, we present an overview of experimental, simulation, and theoretical results that probe multi-scale polymer and nanoparticle dynamics in polymer nanocomposites and navigate the dense parameter space presented by these multicomponent systems. Although a variety of PNC systems are mentioned, we focus this discussion on linear thermoplastics filled with hard spherical or cylindrical NPs in the melt state. We begin by introducing PNCs, the dynamic processes within them, and the importance of dynamics for properties and processing. At the smallest length and time scales, we discuss segmental dynamics in PNCs, including the role of polymer attributes, NP attributes, and NP-polymer interactions. Then, we present measurements of collective motions and intermediate (Rouse) dynamics in various PNC materials. At longer length and time scales, we discuss polymer center-of-mass diffusion in PNCs with either spherical or anisotropic NPs. We then explore the dynamics of the NPs in PNCs and polymer melts, including theoretical predictions, simulation results, and experimental observations. Finally, we note some of the remaining challenges in probing dynamics in PNC materials and fundamentally studying PNCs more generally.

Selected Abbreviations: b, Kuhn length of the polymer segments; BDS, broadband dielectric spectroscopy; BLL, bound loop layer; D, polymer diffusion coefficient (in PNC); D_0, neat polymer diffusion coefficient; d_{app}, apparent tube diameter; DIL, dynamic interfacial layer; DLS, dynamics light scattering; DMA, dynamic mechanical analysis; DSC, differential scanning calorimetry; D_{SE}, Stokes Einstein diffusion coefficient; d_{tube}, entanglement tube diameter; ERD, elastic recoil detection; FCS, flourescent correlation spectroscopy; ID, interparticle separation distance; ISF, intermediate scattering function; L, NP length; LJ, Leonard Jones; MD, molecular dynamics; MSD and $<r^2>$, mean squared displacement; M_w, molecular weight; N, degree of polymerization; N_e, degree of polymerization between entanglements; NMR, nuclear magnetic resonance; NPs, nanoparticles; NR, neutron reflectivity; NSE, neutron spin echo spectroscopy; OAPS, octaaminophenyl polyhedral oligomeric silsesquioxane; P2VP, poly(2-vinylpyridine); PBMA, poly(butyl methacrylate); PDMS, polydimethylsiloxane; PEG, polyethylene glycol; PEO, polyethylene oxide; PEP, poly(ethylene–propylene); PIm, polyimide; PMA, poly(methylacrylate); PMMA, poly(methyl methacrylate); PMP, poly(4-methyl-2-pentyne); PNCs, polymer nanocomposites; PP, polypropylene; PPG, polypropylene glycol; PS, polystyrene; PVAc, polyvinyl acetate; PVME, poly(vinyl methyl ether); q, scattering wave vector; QENS, quasi-elastic neutron scattering; RBS, Rutherford backscattering spectrometry; R_g, polymer radius of gyration; R_{NP}, nanoparticle radius; S(q,ω), dynamic structure factor; SCGLE, self-consistent generalized Langevin equation; SIMS, secondary ion mass spectroscopy; SiO_2, silica; SPT, single particle tracking; T, temperature; T_g, glass transition temperature; TMDSC, temperature modulated differential scanning calorimetry; VFT, Vogel-Fulcher-Tammann; Wl^4, Rouse parameter; XPCS, X-ray photon correlation spectroscopy; τ_α, relaxation time of α-process; ΔC_p, the step in heat capacity; α-process, primary structural relaxation process; ε, LJ interaction strength; φ_{NP}, NP volume fraction; η, viscosity; η_0, zero-shear viscosity; σ, unit length-scale for simulations; σ_{graft}, surface grafting density; τ, relaxation time (general); τ_0, elementary (Kuhn segment) relaxation time; τ_e, entanglement relaxation time; τ_t, terminal relaxation time; ω, frequency.

* Corresponding authors.
E-mail addresses: ebailey@seas.upenn.edu (E.J. Bailey), winey@seas.upenn.edu (K.I. Winey).

https://doi.org/10.1016/j.progpolymsci.2020.101242
0079-6700/

Contents

1. Introduction

Polymer nanocomposites (PNCs), or materials comprised of nano-sized fillers embedded in a polymer matrix, have generated substantial academic and industrial attention in recent decades. Compared to composites with micron-sized fillers, the use of nanoparticles (NPs) drastically increases the NP-polymer interfacial area and decreases NP-NP separations at the same concentration of filler [1,2]. As such, a resulting PNC can have drastically different properties as compared to the host matrix or traditional composites. In fact, these different properties can be varied, controlled, and tuned using the broad set of parameters that these hybrid materials offer. These parameters include those associated with the NP (size, shape, and surface), polymer (molecular weight, chemistry, and architecture), and PNC (concentration, NP-polymer interaction, and NP dispersion state). In addition, inclusion of the NP can add functionality including electrical, plasmonic, barrier, or stimuli-responsive properties to a polymer matrix otherwise devoid of those properties. Importantly, many PNCs still maintain the favorable properties of the polymer such as processability and low mass density.

Polymer nanocomposites are exciting candidates for a variety of applications and industries, as reviewed by others [3–12]. Early interest in nanoparticle-filled polymers was primarily for car tires, where NPs are added to rubber to increase strength, wear resistance, and traction while maintaining low cost and weight [4]. Similar properties make PNCs desirable for different applications, including various parts in ground and air transportation and sports equipment. In addition, PNCs have desirable barrier, permeability, and selectivity properties making them ideal candidates for membrane and separation technologies such as gas separation, water filtration, and food packaging [7,13]. For example, the addition of fumed silica NPs with poly(4-methyl-2-pentyne) (PMP) resulting in substantial increases in both n-butane permeability and n-butane/methane selectivity, two parameters that often compete with each other [14]. The addition of NPs can also add functional properties, especially optic and electronic properties, to the polymer matrices. The most common example is the augmentation of electrical conductivity to an otherwise insulating polymer matrix through the inclusion of a percolated network of silver nanowires, carbon nanotubes, or other conductive fillers [15–18]. Similarly, the addition of plasmonic or upconverting NPs to a polymer matrix has been used to realize optoelectronic applications and or to enhance the efficiency of solar cells [10,12,19].

Despite the appealing properties that have been observed, much remains unknown, especially regarding PNCs more fundamentally. In this vein, this review will broadly survey and discuss recent studies of multiscale polymer dynamics and NP dynamics in polymer nanocomposites, as depicted in Fig. 1. As discussed in Section 2, PNCs exhibit several different dynamic processes that are interrelated and dictate or influence properties and performance. In subsequent sections, we will discuss and review selected theoretical, simulation, and experimental approaches and studies as they pertain to the different dynamic processes. Beginning at the shortest length and timescales, Section 3 will explore polymer segmental dynamics in PNCs, followed by non-diffusive polymer chain relaxations (intermediate dynamics, Section 4), center-of-mass polymer diffusion through PNCs (Section 5), and NP dynamics in polymer and PNC melts (Section 6). Finally, Section 7 will provide an outlook and will discuss outstanding scientific challenges regarding the dynamics of polymers and nanoparticles in PNCs.

This review will generally focus on model PNCs systems of linear thermoplastics filled with hard nanoparticles in the melt state, although in some cases, other relevant systems will be discussed. Although many different polymers and fillers will be discussed, the

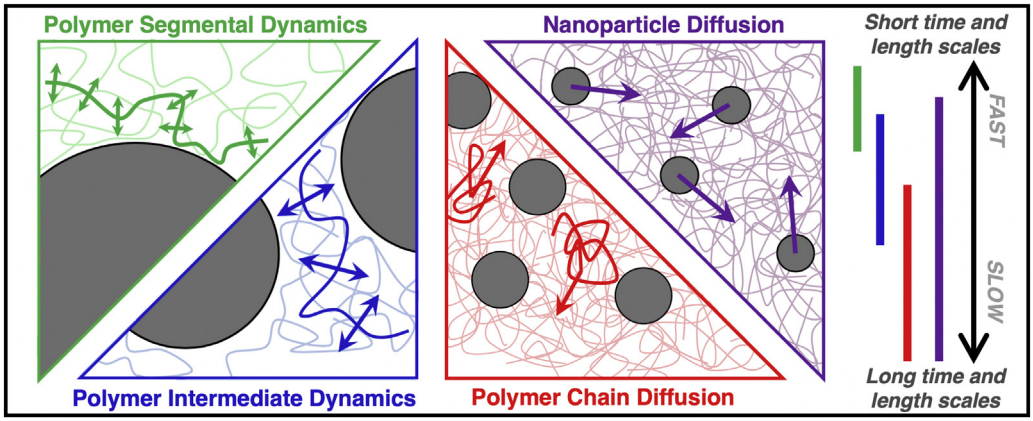

Fig. 1. Schematic to highlight the time- and length-scales of various dynamic processes in polymer nanocomposites (PNCs).

majority will be inorganic metallic and ceramic nanoparticles. PNCs with silicates and carbon-materials (CNTs, C60, graphene, carbon black) have been reviewed elsewhere [16,20–24] and will receive only cursory mention in this review. More focused reviews regarding various classes of PNCs or aspects of dynamics may also be of interest [25–34].

2. The importance of dynamics in polymer nanocomposites

2.1. Overview of dynamics processes in polymer nanocomposites

Polymer melts have a rich hierarchy of time- and length-scale dependent dynamic processes [35]. At the smallest time-scales and sub-angstrom length-scales, atoms in a solid undergo thermal vibrations at finite temperature. These fast dynamics are often on the pico-second time scale and are characterized by particles rattling in cages formed by the local packing of nearby atoms. Generally, these fast dynamics are unaffected by the connectivity of monomers that is characteristic to polymer chains, except when the molecular weight (M_w) affects the local packing. Unlike longer length-scale dynamics, these local relaxations may be active even when the temperature (T) is less than the glass transition temperature (T_g). This review will not discuss these local, fast dynamics.

Segmental dynamics occur at various time-scales and at length-scales at or below those associated with a Kuhn segment. Broadly, segmental dynamics can be defined as the non-diffusive relaxations of a group of bonded atoms within a polymer chain. The α-process is the primary structural relaxation that refers to the cooperative reorientation and conformational fluctuations of a set of adjacent monomers along the polymer backbone. The glass transition temperature of a polymer can be defined dynamically through the arrest of this α-process or thermodynamically through changes in thermodynamic properties (such as density, thermal expansion coefficient, or heat capacity) [36]. At smaller length scales within a Kuhn segment and generally faster timescales, secondary relaxations (β, γ, etc.) occur in some polymers. These relaxations are often associated with motions of side groups as opposed to the backbone, especially for bulky, flexible, or complex repeat units. For example, several secondary relaxations have been identified in polystyrene (PS) melts both above and below T_g [37]. In general, this review will focus on the α-process when discussing segmental dynamics in PNCs.

The dynamics at time- and length-scales beyond segmental dynamics are the those associated with the polymer chains, which include non-diffusive relaxations or translational diffusion, and are therefore on the order of or less than the radius of gyration (R_g) of the chain. The Rouse model is used to describe the dynamics of chain sections (modes) of arbitrary length in the melt, while the Zimm model is the analogous theory for polymers in solution [35]. For sufficiently short polymers, the Rouse model extends to describe the translational diffusion coefficient of the entire chain. However, as the degree of polymerization increases, chains in the melt eventually interpenetrate and form topological constraints known as entanglements. For entangled polymer melts, Rouse dynamics describe the relaxation of Rouse modes between entanglements, but no longer apply to chain-level dynamics when the relaxations are restricted by the entanglement network. For an entangled chain to fully relax and diffuse, it must either diffuse through the entanglement network through a process called reptation or the entanglement network must relax to no longer impede the chain motion through a process called constraint release [35]. Reptation refers to the process by which segmental relaxations and friction within the confining tube (following Edwards tube theory) lead to chain translocation along the contour length through the entanglement nodes. Whether the an unentangled chain diffuses via Rouse motion or an entangled chain diffuses via reptation, the dynamics are characterized by the center-of-mass diffusion coefficient (D).

When considering polymer nanocomposites, it is important to note that the sizes of NPs are similar to or smaller than the characteristic size of polymers (R_g). As such, the relaxational and motional processes of NPs and polymers often have overlapping time-, energy-, and length-scales. To be specific, NP motion is considered a competition between thermally-driven kinetic forces that promote NP diffusion and viscous drag forces from the polymer medium that slow the NP diffusion, qualitatively similar to Stokes-Einstein [38]. However, as will be discussed in Section 6, the molecular origin of these forces depends on the time-, energy-, and length-scales of the NPs and polymer medium. In addition, at small length scales, NPs can exhibit non-diffusive relaxation dynamics, including rattling in the local environment, ballistic motion, and in the case of anisotropic NPs, reorientation fluctuations.

2.2. Polymer nanocomposites properties dictated by dynamics

The microscopic dynamics of polymers and NPs are critically important to understand, design, develop, and fabricate new PNCs. The dynamic processes discussed in Section 2.1 often influence or even dictate various macroscopic properties and the processability of PNCs. Thus, fundamental studies of dynamics, like those

discussed herein, in these materials are essential to realize next generation technologies and to mass produce PNCs cost effectively. This is not to say dynamic properties are the only barrier to widespread PNC development and application. In fact, other recent reviews have highlighted other critical aspects of PNC research [2,4,9,12,25,33], but many others have noted the importance of dynamics [25–29].

Polymer dynamics in melts and nanocomposites are critical for various macroscopic PNC properties, so understanding and documenting the polymer dynamics can help predict, control, and understand the final PNC performance. For example, mechanical properties including stiffness, strength, and stress relaxation are known to be influenced by segmental dynamics. Slow secondary segmental relaxations in the glassy state lead to enhanced mechanical stiffness and slower dynamics in the melt can increase the melt viscosity. In fact, the addition of NPs can controllably alter segmental dynamics and therefore control various mechanical properties [39–41]. In addition, segmental mobility often dictates transport properties, including ion transport for energy applications [42] and small molecule transport for membrane and separation technology [7,14,43–45]. For example, enhanced permeability of CO_2 was observed at an intermediate grafting molecular weight in matrix-free PNCs comprised of silica (SiO_2)-grafted poly(methylacrylate) (PMA) [43], and this behavior was correlated to increased local free volume and faster segmental dynamics [46].

Dynamics in PNCs can also lead directly to unique and functional properties, including stimuli-responsive and self-healing properties [47–49]. For example, multilayer films comprised of flexible polymer and brittle oxides are common in electronic components for various industries, but suffer from crack formation and propagation. However, if the polymer is replaced with a PNC, the NPs can be engineered to diffuse into cracks to provide self-healing properties and achieve improved durability [48]. Similar responsive properties can be used to make advanced sensors and other responsive materials.

The appealing properties that have been reported for small batches of PNCs, cannot be ubiquitously deployed until the PNCs can be manufactured cost-effectively in mass quantities. Importantly, the dynamic processes in PNC materials can inform or guide processing routes and parameters necessary for mass production. For example, melt processing and molding requires flow of the PNC material, which is related to the chain-scale dynamics. After processing, the NP morphology is often metastable, so understanding how rapidly a PNC evolves is necessary to maintain the metastable condition, if desirable, or achieve equilibrium. When a random NP dispersion is desired in the glassy state and NPs tend to aggregate in the melt state, then precise knowledge of polymer chain and NP dynamics allows engineers to properly design the process protocols. Furthermore, NPs can be added to enhance the manufacturability of materials by either enhancing dynamics and rheology (i.e. a plasticizer or diluent) or slowing dynamics (i.e. an anti-plasticizer).

Polymer nanocomposites are also model systems to understand multicomponent systems with related physics. For example, the large surface area to volume ratio of NPs increases the amount of interfacial polymer. Thus, systematic studies of well-defined PNCs can probe the structure and dynamics of polymers near interfaces [31,50]. Similar effects can be studied at solid and flat interfaces, but these thin films suffer from weak signal, because comparatively fewer polymer chains are at the interface. In addition, PNCs (especially those with entangled polymers) are a model system that can be used for understanding diffusion of NPs and molecules in complex media, such as biological tissue and other organic matter [26,51–53]. As such, understanding the dynamics in PNCs can provide insights into other, more complicated systems.

3. Polymer segmental dynamics

3.1. Experimental and simulation methods

For $T>T_g$, polymer segments cooperatively relax and reorient in the melt. For the primary structural relaxation process (α-process), the relaxation time (τ_α) follows Vogel-Fulcher-Tammann (VFT) behavior:

$$\tau_\alpha(T) = \tau_\infty \exp\left(\frac{B}{T - T_0}\right) \quad (1)$$

where τ_∞, B, and T_0 are fitting parameters related to high temperature relaxation time, fragility, and Vogel temperature, respectively [35]. As shown in Fig. 2, the segmental relaxation time (α-process) can be probed with a variety of experimental techniques, each of which has a unique temporal range and corresponding temperature for a given polymer [36,54,55]. Furthermore, as will be discussed in subsequent sections, each technique samples the material and population of dynamics differently.

When the relaxation time is slow ($\tau > \sim 1$ s) at $T \sim T_g$, temperature modulated differential scanning calorimetry (TMDSC) can be used to measure segmental dynamics, as described elsewhere [54,56]. Differential scanning calorimetry (DSC) characterizes the glass transition temperature by monitoring the change in heat capacity, which reflects changes in polymer configurational degrees of freedom upon heating or cooling a polymer sample [36]. Similarly, TMDSC monitors heat capacity upon heating or cooling with a superimposed sinusoidal function to separate the reversible and non-reversible heat flows to improve sensitivity, resolution, and isolation of overlapping transitions [56]. Although T_g is dynamically defined as the temperature at which the α-process becomes infinitely slow, it is often used as a proxy for segmental dynamics whereby an increase in T_g is attributed to slowing of the α-relaxation process [36].

For faster dynamics ($\tau \sim 10^{-7}$–10^{0} s) at $T>T_g$, broadband dielectric spectroscopy (BDS) offers a broad dynamic window over which molecular dynamics can be probed. As detailed elsewhere [57],

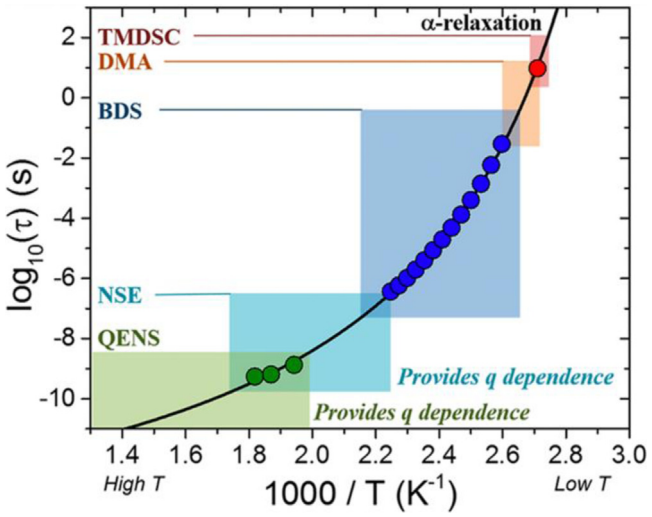

Fig. 2. Primary segmental relaxation times (α-process) of bulk 40 kg/mol P2VP as a function of inverse temperature. Shaded regions depict the approximate time scales and their corresponding temperature scale for five techniques: temperature-modulated differential scanning calorimetry (TMDSC), dynamic mechanical analysis (DMA), broadband dielectric spectroscopy (BDS), neutron spin echo (NSE), and quasi-elastic neutron scattering (QENS). Black line represents a VFT fit for TMDSC (red circle), BDS (blue circles), and QENS (green circles) measurements of neat P2VP [55]. Copyright 2019. (For interpretation of the references to color in this figure legend, the reader is referred to the web version of this article.)

Reproduced with permission from the American Chemical Society.

BDS applies a sinusoidal electric field to the sample and precisely measures the complex impedance, which is converted to dielectric permittivity, as a function of frequency of the oscillating field. Encoded in the BDS spectra are the timescales associated with reorientations of unpolarized dipole moments along or pendent to the chain as well as the movement of free ions in the sample [57]. Limitations of BDS include an insensitivity to length-scales, the requirement for a permanent dipole on the polymer, and somewhat complicated fitting [58]. Conversely, the benefits to BDS include a broad frequency range, high accuracy and precision, and a measurement of the fraction of relaxing dipoles through the integrated amplitude.

For fast segmental dynamics ($\tau \sim 10^{-11}$–10^{-6} s) at $T \gg T_g$, inelastic neutron scattering such as neutron spin echo spectroscopy (NSE) and quasi-elastic neutron scattering (QENS) can characterize polymer segmental relaxations and, importantly, simultaneously provide length-scale information. In both measurements, the distribution of neutron energies is measured after scattering from the sample as a function of the wave vector, q. Since neutrons and molecular motions are on the μeV range, scattered neutrons gain or lose energy during a scattering event with mobile species and elastically scatter with atoms immobile on the experimental timescale [59,60]. NSE is commonly used for intermediate dynamics (Rouse) so it will be more thoroughly discussed in Section 4.1. For QENS, time-of-flight and backscattering approaches precisely measure the broadening of the elastic scattering peak. This dynamic structure factor, S(q,ω), is often dominated by hydrogen atoms in the sample due to their large neutron scattering cross-section and can be fit to reveal the molecular relaxation times as a function of q. Although instrument access and data analysis can be challenging, QENS is unique in that it simultaneously probes the length- and time-scales to thoroughly study motions and allows H/D labelling to delineate inter- or intrachain dynamics.

Additional experimental techniques exist for characterizing the segmental dynamics in PNCs. Dynamic mechanical analysis (DMA) and rheology are mechanical measurements that can probe the dynamics of segments, and like NSE, can address intermediate polymer dynamics (see Section 4.1). Nuclear magnetic resonance (NMR) is not pictured in Fig. 2 but can measure segmental dynamics over various timescales with various techniques [54,61,62]. Most relevant to PNC segmental dynamics are measurements of proton spin-spin relaxation times (T_2) from spin echoes pulse sequences. The proton relaxation curves are usually fit to a function comprised of several contributions for different phases of segmental mobility. Most commonly, fits are comprised of three phases: an apparently immobile glassy phase attributed to segments adjacent to the NP, a phase of reduced mobility attributed to relaxations in proximity to the NP, and a bulk-like phase attributed to free polymer segments.

Computer simulations, namely molecular dynamics (MD) simulations, are often used to probe segmental dynamics as well. In many cases, the dynamics of segments can be observed in fully atomistic MD simulations. Due to computational expense, atomistic MD simulations are often restricted to low M_w, small NPs, and short (fast) dynamics. Coarse-graining atoms into segments (or beads) and accordingly altering atomic potentials is often done to reduce simulation time and access slower dynamics and longer length-scales. A common model used to study fundamental polymer physics is the Kremer-Grest model wherein non-bonded beads interact through a pairwise Leonard Jones (LJ) potential and bonded beads interact via a harmonic spring [63]. The NP-polymer interaction in PNCs is also often modelled with an LJ potential. Generally, each bead in these simulations represents at least a few monomers and less than a Kuhn segment when compared to experiments. With a record of atom or bead coordinates as a function of time, several different analysis routes (including bond correlations, intermediate scattering function (ISF), and mean-squared-displacement (MSD)) lead to insights regarding the time-scales and mechanisms of segmental motion in atomistic and coarse-grained polymer melts.

3.2. Heterogenous segmental dynamics in attractive PNCs

Segmental dynamics occur over small length scales (within a few nanometers), are sensitive to the local polymeric environment, and are affected by cooperativity and local free volume. Thus, polymer melts exhibit a distribution of relaxation times in the melt state. PNCs exhibit an even broader distribution of segmental relaxation times, because spatial heterogeneities exist and dynamics near NP surfaces differ from those far from NPs. With this in mind, there are three general models used to describe dynamics in PNCs, Fig. 3. The simplest model is the homogeneous model, where the average relaxation time measured is assumed to be the relaxation

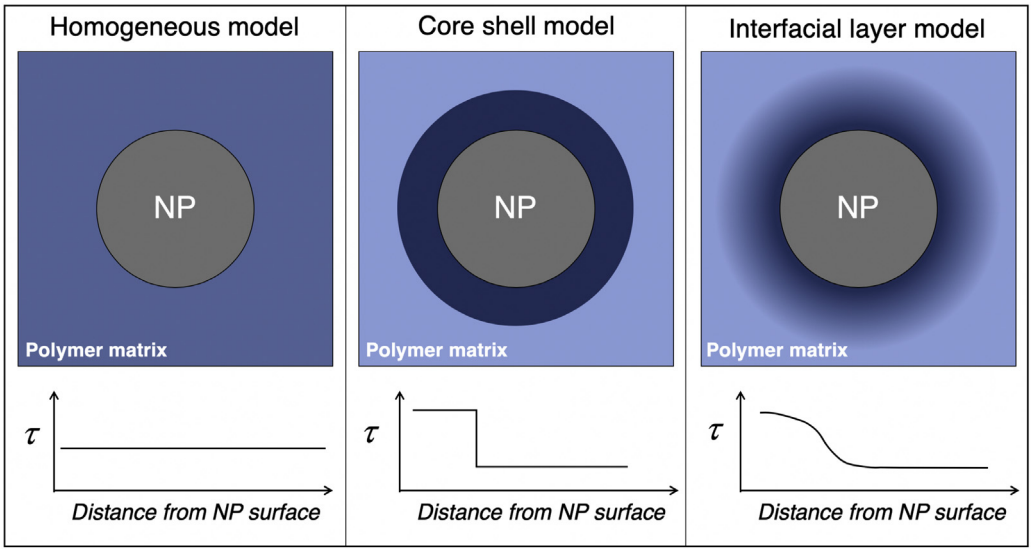

Fig. 3. Schematic showing polymer segmental dynamics as a function of distance from a single NP. The homogeneous model (left) assumes an average relaxation time throughout the polymer matrix. The core-shell model (center) spatially separates the polymer relaxations into a slower population adjacent to the NP and another bulk-like population away from the NP surface. The interfacial layer model (right) assumes a distribution of relaxation times that decreases smoothly from the NP surface into the matrix.

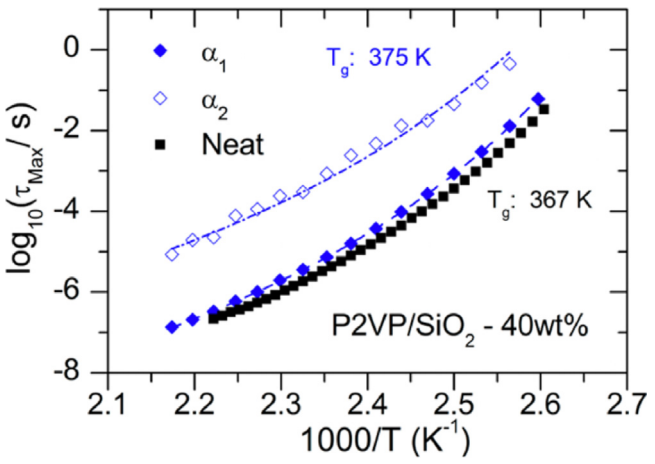

Fig. 4. Mean molecular relaxation time (τ_{Max}) as a function of inverse temperature for neat poly(2-vinylpyridine) (black squares) and P2VP segments in P2VP/SiO_2 PNCs (φ_{NP} = ~26 vol%, blue). Relaxation times in the PNC are separated and plotted as interfacial relaxations (blue open diamonds) and bulk-like relaxations (blue filled diamonds) [65]. Copyright 2014.

Reproduced with permission from the American Chemical Society.

time for all segments in a PNC. The core-shell model simply has two populations of relaxations, namely those near and far from NP surfaces, the latter of which normally relax at timescales similar to bulk. Finally, the interfacial layer model is similar to the core shell model, but the transition from interfacial relaxations to bulk-like relaxations is smooth rather than stepwise, and therefore assumes some functional form. Naturally, details of the PNCs system, such as the NP-polymer interactions, NP size (R_{NP}), and NP volume fraction (φ_{NP}), influence which model is most appropriate to describe the population of segmental dynamics. Similarly, some measurement methods permit the use of different models whereas other methods restrict the analysis to a single model. For example, it is possible to use any model in Fig. 3 to interpret BDS measurements of well-dispersed NPs because the broad frequency range surveys the full distribution of relaxation times. Conversely, for measurements with less precision and a smaller temporal window, the homogeneous model may be the only option due to the difficulties associated with separating multiple relaxations. We also note that heterogeneities displayed in Fig. 3 can be observed in the form of a distribution of relaxation times through stretching or shape parameters, most commonly in BDS and QENS using Havriliak–Negami (HN) and Kohlrausch–Williams–Watts (KWW) functions to describe experimental data.

It is well-established that the addition of well-dispersed attractive NPs to a polymer melt (for $R_g \sim R_{NP}$) slows segmental dynamics as a function of NP loading (i.e. NP-polymer interfacial area). To demonstrate and understand this effect, several authors have studied the model system of poly(2-vinylpyridine) (P2VP) mixed with colloidal silica (SiO_2) and measured segmental relaxations with TMDSC [64,65], BDS [65–67], and QENS [55]. In this system, hydrogen bonding between pyridine in P2VP and hydroxyls on the surface of SiO_2 NPs leads to a strong NP-polymer interaction (estimated to be on the order of ~10 k_BT) [64,68,69].

Using the core-shell model and combining TMDSC, BDS, and small-angle X-ray scattering (SAXS), Sokolov and coworkers revealed a shell of slow P2VP segmental dynamics at the P2VP/SiO_2 interface [65]. A single Havriliak–Negami (HN) function [57] was unable to capture the broad distribution of α-relaxations in the PNC, so two HN functions were used and attributed to bulk-like relaxations far from the NP surface (α_1) and slower relaxations near the NP-polymer interface (α_2). The extracted relaxation times reveal three important observations (Fig. 4): (i) α_1 relaxations far from the NP interface are approximately bulk-like, (ii) α_2 relaxations near the NP interface are ~100 times slower than bulk, and (iii) the temperature dependence of α_1, α_2, and neat P2VP are comparable although α_2 relaxations have a slightly weaker temperature dependence [65]. Using the dielectric strength of each process as a measurement of the amount of relaxing polymer, the authors estimate a shell thickness on the order of ~4 nm, which is between the Kuhn size and R_g of P2VP and matches structural measurements from SAXS. In addition the authors observe that all segments are mobile, albeit many are slow, which is in contrast to other reports that discuss and immobile polymer layer [68,70,71]. It is worth noting that simpler and more sophisticated models have been used to describe BDS data from various PNC systems [58,66,72,73], and they all result in observations of slow interfacial relaxations within a few nanometers of the NPs. Fitting the same BDS data with a core shell model (two HN functions) results in a thinner apparent bound layer and apparently slower interfacial relaxations as compared to fitting with the interfacial layer model, but both qualitatively show slow interfacial dynamics [73].

Similarly slow dynamics have been measured in P2VP/SiO_2 nanocomposites using TMDSC [64,65,74] and QENS [55]. The simplest analysis of TMDSC assumes a single glass transition like the homogeneous model [64], but more detailed analysis reveals high temperature broadening (i.e. slower dynamics) [65] and even can lead to extraction of an interfacial layer thickness that is commensurate with BDS [73,74]. QENS measurements on neat P2VP showed diffusive motions ($\tau \sim q^{-2}$) for length- and time- scales of ~1 nm and ~1 ns, which agreed with extrapolations of the α-process from TMDSC and BDS in neat P2VP (Fig. 2) [55]. In P2VP/SiO_2 PNCs these relaxations occurred with a similar q-dependence but at slower timescales than bulk and timescales monotonically decreased with NP loading (i.e. NP-polymer interfacial area) [55]. This result implies, at least preliminarily, that segments are perturbed temporally more than spatially.

This case study of segmental dynamics in P2VP/SiO_2 PNCs demonstrates the sensitivity of experimental observations to the measurement technique, data interpretation, and measurement conditions, although this is not specific to the P2VP system. Each experimental technique has different sensitivities, dynamic ranges, and probes the population of relaxation times differently, all of which may lead to distinct experimental observations. For example, TMDSC fundamentally measures the freezing out of modes of motion near T_g, and samples all segments evenly [29,56,75]. In contrast, QENS is measured at $T \gg T_g$, fundamentally measures the incoherent dynamic structure factor, and it's sampling is nontrivial [55,76,77]. As discussed in Section 7, extreme care should be used when comparing different PNC systems and measurement techniques. Nevertheless, Sections 3.3–3.5 aim to compare the effect of different PNC parameters using a combination of experimental methods, material systems, and simulations.

Finally, it is worth noting that several reports have suggested analogies between polymer nanocomposites and thin film confinement [50,68,78–80], polymer confined to nanopores [26,31,81–83], and intercalated systems [23,24,84]. In thin polymer films for example, T_g can change drastically as a function of film thickness (up to ~100 nm) depending on the substrate-polymer interaction and the presence of a free surface [85–87]. The most realistic comparison here is between PNCs with strong confinement, i.e. where the interparticle distance (ID) is smaller than the chain size ($2R_g$), and thin films capped on both ends by a rigid substrate [31,36]. However, the role of NP curvature and the subsequent heterogenous levels of confinement between spherical NPs in PNCs cannot be ignored [80]. Nevertheless, several concepts demonstrated and learned in thin films, as well as infiltrated nanopores and PNC systems with silicates, can be extended this discussion and vice versa.

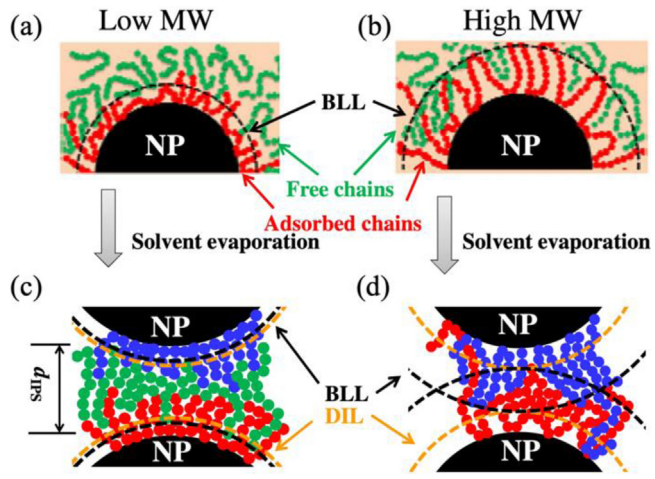

Fig. 5. Schematic representation of the MW effect in PNCs with attractive NP-polymer interactions. (a) and (c) Nanoparticles in polymer solutions with free (green) and adsorbed (red) chains. (b) and (d) Polymer nanocomposites formed by solvent evaporation with free (green) and adsorbed (blue and red) polymers. For PNCs with low M_w, the bound chains are compact resulting in a similar BLL (bound loop layer) and DIL (dynamic interfacial layer) and overall slower segmental dynamics than PNCs with higher M_w with larger BLL than DIL [73]. Copyright 2016. (For interpretation of the references to color in this figure legend, the reader is referred to the web version of this article.)

Adapted with permission from the American Physical Society.

3.3. *Effect of polymer attributes*

Several inherent parameters to the polymer can affect the dynamics in PNCs and the perturbation imposed by the NPs, including but not limited to molecular weight, polymer stiffness, and polymer architecture. This section reviews how changes to these properties affect the segmental dynamics in PNCs.

Although segmental dynamics in neat polymer are nearly independent of M_w for $M_w \gg M_0$, the substantial presence of interfaces in PNCs and the relative size of the NPs lead to different perturbations based on matrix molecular weight. Detailed BDS and TMDSC measurements on poly(vinyl acetate) (PVAc)/SiO_2 and P2VP/SiO_2 PNCs found the magnitude that segmental dynamics were slowed relative to neat polymer and the length-scale over which they were perturbed increased with decreasing M_w [73]. In other words, the perturbation imposed by the NPs was stronger with low M_w polymer as compared to large M_w. The authors describe this behavior in terms of interfacial packing and bound layer density, as supported by SAXS, spectroscopy, and mass density measurements [69,73], Fig. 5. Specifically, low molecular weight polymers are proposed to adsorb more densely (forming more trains than loops or tails) as compared to higher molecular weight. This difference in polymer conformations leads to more adsorbed segments and more suppressed dynamics in PNCs with lower molecular weight. In addition, the dynamic interfacial layer (DIL) defined by slow interfacial dynamics and bound loop layer (BLL) as defined by structural measurements are similar for low M_w, while the BLL is thicker than the DIL for high M_w. A similar molecular weight effect was observed in other experiments as well [39,55,88]. In contrast, NMR studies on segmental dynamics in polyethylene glycol and SiO_2 PNCs observed a weak M_w-dependence where the fraction of slow segments increased with M_w [89] or remained the same [70]. These differences could be attributed to weaker polymer-NP interactions or other experimental system-specific parameters.

It remains unclear if the structure and polymer conformations proposed in Fig. 5 are at equilibrium or kinetically trapped and therefore depend on PNC processing (as further discussed in Section 7). In fact, the bound layer thickness and fraction of immobilized segments were recently measured via NMR in PEO/SiO_2 PNCs fabricated from different solvents [70]. PNCs fabricated from a poor solvent (ethanol) produced more adsorbed segments and a thicker bound layer than those fabricated from a good solvent (water) and this effect was observed at two molecular weights [70]. These measurements show that the bound layer structure and dynamics depend on the processing conditions, indicating the polymer chains and PNCs in general are not at a global equilibrium state in the melt. Interestingly, the M_w-effect captured in Fig. 5 persisted after annealing for $\sim 10^{14}$ τ_α, meaning the effect (if not at equilibrium) is long-lasting and thermally stable [73]. However, in a different study of P2VP/SiO_2 PNCs, a similar M_w-dependence was observed in TMDSC ($T \sim T_g$), while only a modest M_w-dependence was found in QENS ($T \gg T_g$) [55]. More measurements are needed to determine if these differences are the result of relaxations toward equilibrium at sufficiently high temperatures, differences in the bound layer as a function of temperature, or simply differences in precision and uncertainty in the different techniques.

Next, we consider matrix-free PNCs comprised of only polymer grafted NPs and specifically consider the molecular weight dependence [46,88,90–92]. One may expect grafted polymer chains to have reduced mobility compared to neat polymer because one end of the chain is covalently bonded to the NP surface and therefore immobile. Grafted PS [90] and P2VP [88] chains have higher T_g (slower dynamics) than neat polymer of the same M_w. Shorter grafts exhibit larger differences relative to neat PS in the breadth of the glass transition, the step in heat capacity (ΔC_p), and fragility because a larger fraction of the chain is near the surface [90]. However, the NP concentration in matrix-free PNCs (and NP-NP separation distance) depends on the M_w of the grafted polymer, the surface grafting density (σ_{graft}), and the NP size, thus complicating comparisons. As such, it is important to consider the conformations of the grafted chains that lead to non-monotonic behavior with M_w [5,46,88]. For example in P2VP/SiO_2 matrix-free PNCs measured by BDS, P2VP segments in low M_w grafts are slower than bulk because each segment resides near a NP and chain stretching impedes relaxations but segments in high M_w grafts exhibit bulk-like relaxations because most segments are far from the NP surface and interfacial effects are less significant [88]. In PMA/SiO_2 matrix free PNCs measured by QENS and assuming a jump diffusion model, segmental diffusion is faster than bulk for all M_w, consistent with increased free volume [46]. Interestingly, the fastest relaxations are measured at intermediate M_w, which are long enough for chains to begin to interdigitate with neighboring NPs and short enough so that the majority of segments are still near NP cores [46]. In matrix-free PNCs of grafted NPs more generally, it is important to consider the brush conformations as a function of M_w, σ_{graft}, and R_{NP} because different dynamics are expected for different conditions. Systematic studies showing these complicated effects are necessary but remain synthetically and experimentally challenging.

Another polymer characteristic that has a profound effect on segmental dynamics in PNCs is the chain stiffness, likely because it strongly affects interfacial packing. In coarse-grained MD simulations, the polymer chain stiffness was controlled by adjusting bending potential (without changing other polymer or PNC parameters) and the dynamics were measured near a flat attractive substrate which simulates an infinitely large NP [93]. The segmental dynamics of chains near the interface were slower than bulk regardless of stiffness but the degree of slowing and length scale over which chains were perturbed both increased for stiffer chains [93]. Isolating the chain stiffness experimentally is challenging because changing the polymer chemistry also changes the NP-polymer interaction, a variable discussed in Section 3.5. Nevertheless, Sokolov and coworkers surveyed the DIL in SiO_2 PNCs with

polypropylene glycol (PPG), PVAc, P2VP, and in literature to reveal qualitatively similar dependencies as simulations [74]. This result suggests that the structure and dynamics of the interfacial polymer layer are impacted by the persistence length and cooperativity of the polymer. More simulations and experiments could further develop the understanding of this relationship.

3.4. Effect of filler attributes

A common parameter to study in PNCs is the relative amount of polymer and filler, which effectively increases the NP-polymer interfacial area. In addition, in certain PNC systems especially at sufficiently high NP concentrations, NP-NP aggregation and polymer bridging between adjacent NPs produce non-trivial effects on segmental dynamics. The case of NP aggregation can often be considered in terms of NP-polymer interfacial area because aggregated NPs have considerably less accessible surface area to the matrix (per unit volume NP) than individually dispersed NPs. As a result, segmental dynamics are generally less perturbed in aggregated PNCs compared to those with the same volume fraction of individually dispersed NPs [71,94,95].

In PNCs with spherical NPs that are individually and randomly dispersed in a polymer melt, the interparticle separation distance (ID) [96] can be expressed as:

$$ID = d_{NP}\left[\left(2/(\pi\phi_{NP})\right)^{1/3} - 1\right] \quad (2)$$

When ID approaches the chain size ($\sim 2R_g$) polymer bridging between adjacent NPs is observed in simulations and experiments, mainly through mechanical measurements [39,40,97–101]. Although isolating the segmental dynamics in bridging chains is difficult, the segmental dynamics are expected to be more perturbed than non-bridging chains [39,99]. When ID is further reduced toward the Kuhn length of the polymer segments (b), all of the polymers in the PNC are effectively interfacial. For NPs on the order of or larger than 10 nm, this level of confinement ($ID \sim 2R_g$) is difficult to achieve except through unique processing routes [18,102–105], grafted and matrix-free PNCs [106], underfilling [72], layered NP systems, or solvent washing [88,107]. Large changes in T_g measured via ellipsometry [104,105] and segmental dynamics measured via BDS [72,88] have been reported in highly loaded PNCs, but these measurements are challenging due to low signal-noise-ratios.

Another critical parameter of the filler that affects segmental dynamics is the NP size. Note that decreasing the NP size at a fixed NP concentration and random dispersion state increases the NP-polymer interfacial area and decreases ID. Since segmental dynamics are often perturbed at the NP-polymer interface, this implies that smaller NPs will affect more segments in the PNC. Profound differences in segmental dynamics were observed by comparing P2VP filled with SiO_2 NPs ($2R_{NP} \sim 2R_g$) to P2VP filled with octa-aminophenyl polyhedral oligomeric silsesquioxane (OAPS, $2R_{NP} \sim$ b), both of which exhibit favorable NP-polymer interactions, Fig. 6 [108]. In PNCs with small NPs, increasing φ_{NP} increased T_g considerably (reaching ~35 K higher than bulk), while ΔC_p remained unchanged and the fragility of τ_α increased [108,109]. In contrast, PNCs with larger NPs exhibited only weak increases in T_g and fragility and exhibited a linear drop in heat capacity with increased φ_{NP} [108]. These results, supported by corresponding simulation and theory, suggest that small NPs slow segmental relaxations more uniformly, participate in the relaxation process, and perturb segmental dynamics more strongly than larger NPs. However, it should be noted that comparing SiO_2 NPs ($2R_{NP} \sim 25$ nm) and OAPS ($2R_{NP} \sim 1.8$ nm) is extreme. As will be discussed in future sections (including Section 7), the OAPS NPs are mobile on the timescale of polymer relaxations so the contrast between P2VP/SiO_2 and P2VP/OAPS likely reflects the mobility of the NPs rather than the effect of only NP size and curvature [109].

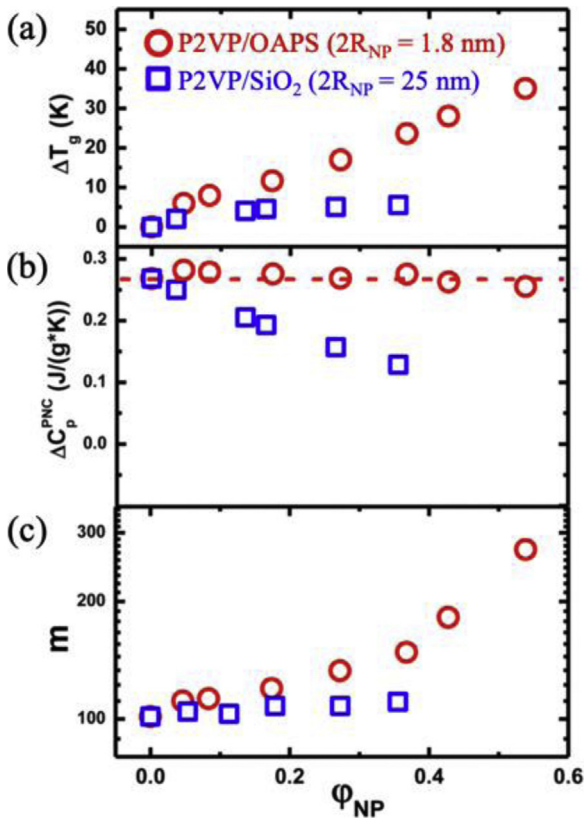

Fig. 6. Effect of NP size in P2VP PNCs with SiO_2 NPs (blue squares, $2R_{NP} = 25$ nm) and octaaminophenyl polyhedral oligomeric silsesquioxane (OAPS) (red circles, $2R_{NP} = 1.8$ nm) as a function of NP volume fraction. (a) Changes in glass transition temperature, $\Delta T_g = T_{g,PNC} - T_{g,bulk}$, (b) magnitude of the step in heat capacity from TMDSC, and (c) fragility [108]. Copyright 2017.
Adapted with permission from the American Chemical Society.

Few studies have isolated the role of NP curvature on segmental dynamics, i.e. systematically changing NP size within the regime of $2R_{NP} >$ b. In a study of P2VP/SiO_2 PNCs with NP diameters ranging from 7 to 50 nm, the bound layer thickness extracted from BDS measurements only slightly increased from 1 to 4 nm [66]. Unfortunately, relaxation dynamics were not reported. Starr and coworkers performed coarse-grained MD simulations of a single facetted icosahedron NP in a melt of low molecular weight polymer to also probe the role of NP size. Here, the segmental relaxations at the interface of a larger NP are slower than near a small NP [80,99]. These authors argue that the relevant parameter to describe changes in T_g is ID relative to R_g, because this captures the convoluted influence of φ_{NP} and R_{NP} and defines the amount of interfacial polymer in the PNC [99]. The infinite limit of NP size is a flat substrate and these comparisons have been discussed [50,78–80]. Still, a universal understanding of how NP size and NP curvature impacts the glass transition and segmental dynamics in PNCs remains elusive, especially experimentally. A combined study that systematically varies NP size (R_{NP}), chain size (R_g), and NP concentration (φ_{NP}) may help characterize the roles NP size relative to ID.

In regard to the shape of the nanoparticle filler, experimental efforts are scarce with the notable exception of carbon-based NPs and clays. Complications include limited availability of non-spherical NPs and changes in NP-polymer interaction with changes in shape. However, we anticipate NP shape to impact segmental dynamics primarily through changes in the local interfacial pack-

ing, local radius of curvature, and amount of polymer-accessible interface. Isolating and deconvoluting these effects remains experimentally challenging.

3.5. Role of NP-polymer interaction on interfacial dynamics

When a polymer is adjacent to a solid interface, such as a NP, the segmental dynamics are affected by several interrelated factors including the differences in density [69,73,80], perturbed polymer conformations [79,110], and the energetics at the interface. Regarding the energetics of a polymer at a NP surface, there is an enthalpic component that characterizes the NP-polymer affinity and an entropic one which characterizes the conformation of free chains near the NP surface. Modulating the NP-polymer interaction enthalpy (through chemical modifications or material selection) or entropy (through interfacial softness or grafting polymer chains to the NP) typically changes other important parameters and therefore complicates experimental comparisons. For example, it is known that the NP-polymer dispersion state depends intimately on the NP-polymer interaction [9,12,97] so it is difficult to deconvolute changes in segmental dynamics from changes in NP-polymer interfacial area. In addition, changing the NP-polymer interaction through materials selection is often accompanied by changes in other important parameters including solvent quality during preparation, chain stiffness, and NP dispersion state.

While many experiments have tried to explore the role of the NP-polymer interaction through altering the NP [84,111–116] or the polymer [64,117], the resulting PNCs frequently have different NP dispersion states and consequently different accessible interfacial area at fixed φ_{NP}. In a thorough study of NP dispersion and glass transition using an array of surface-modified silica and different polymers, Schadler and coworkers argued that NP-polymer energetics and work of adhesion can predict dispersion state of NPs in the melt, as well as the direction and magnitude of T_g changes [118]. Reasonable NP dispersion is achieved when the polymer-NP interaction exceeds the NP-NP interaction and the relative work of adhesion is minimized. In systems with similar dispersion states (characterized by TEM), stronger NP-polymer interactions result in a larger increase in T_g [118]. Measurements of segmental dynamics (rather than the vitrification process) or other characteristics of the bound layer are mostly unreported and present a worthwhile future direction, as discussed in Section 7.1. One way to access interfacial dynamics at repulsive interfaces while circumventing aggregation in PNCs is using infiltrated polymer in nanopores with well-characterized surfaces. For hydrophobic poly(ethylene-alt-propylene) (PEP) infiltrated into hydrophilic anodic aluminum oxide (AAO) nanopores, bulk-like segmental dynamics were measured using neutron scattering [83]. In comparison, hydrophilic polydimethylsiloxane (PDMS) in hydrophilic AAO nanopores (an attractive interaction) displays segmental dynamics slower than bulk [82].

MD simulations of an isolated NP in a polymer melt offer the unique ability to tune NP-polymer interaction without changing other parameters or causing NP-NP aggregation. For example, by extracting the segmental relaxation time as a function of distance from the NP surface for a variety of NP-polymer interactions, Starr and coworkers (Fig. 7) showed slower interfacial relaxations for attractive NPs (ε>1) and faster interfacial relaxations for repulsive NPs (ε<0.5) [119]. The surface relaxation (inset of Fig. 7) reveals surface dynamics between 10^2 times faster and 10^4 times slower than bulk depending on the NP-polymer interaction, with the crossover for bulk-like being slightly more repulsive than athermal. This crossover may indicate an unfavorable entropic effect or an effect of local ordering [119]. This profound effect of NP-polymer interaction on local dynamics is consistent with other simulation results [120–124] but mostly undocumented in experimental PNCs. Interestingly, bulk-like segmental relaxations are recovered after ~3σ, or ~3 nm in experimental units, from the NP surface regardless of NP-polymer interaction parameter [119]. Other simulations have shown similar effects [29,79,121].

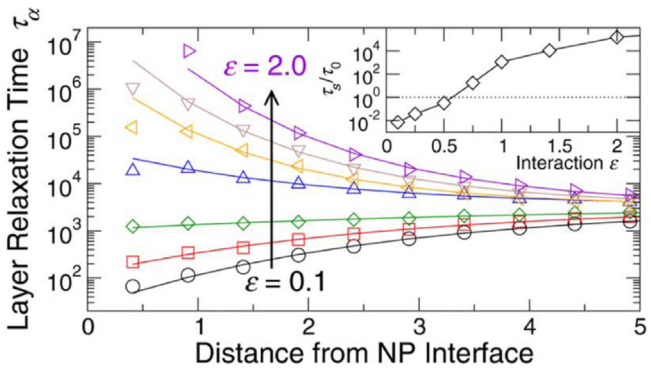

Fig. 7. Segmental relaxation time for ε = 0.1, 0.25, 0.5, 0,75, 1.0, 1.4, and 2.0 as a function of distance from the NP surface. Inset shows surface segmental relaxation time (normalized to that of bulk) as a function of interaction strength [119]. Copyright 2016.

Reproduced with permission from the American Chemical Society.

For systems that exhibit hydrogen bonding, such as PNCs comprised of hydrophilic polymers and SiO_2 NPs, temperature may impact the NP-polymer interaction. Specifically, the relaxation time of adsorbed segments is likely related to the activation energy of the hydrogen bond (relative to kT) and the attempt frequency (related to the bulk relaxation time), both of which are temperature dependent. NMR measurements as a function of temperature showed the measured bound layer thickness in various PNCs decreased with increasing temperatures; unfortunately, measurements of the relaxation time in that bound (glassy) layer were inaccessible [125,126]. Thinner dynamic bound layers were also observed with BDS as temperature increased in a variety of materials [74,123]. As discussed in regards to Figs. 4 and 6, BDS measurements observe only a weak change in fragility upon the addition of NPs with $2R_{NP} > b$ [65,108]. This result may indicate that the NP-polymer interaction is not significantly changed over this temperature range. For $2R_{NP} \sim b$, differences in fragility as T approaches T_g may reflect the frustrated packing during the vitrification process rather than segmental relaxation at higher temperatures [108], meaning the dependence on NP-polymer interaction remains unclear. To access a broader range of temperatures, multiple experimental methods with overlapping temperature ranges is optimal, Fig. 2 [54,55,76,77].

Finally, the role of NP-polymer interaction has also been studied by comparing the segmental dynamics of physically adsorbed chains to those that are covalently grafted to the surface, as mentioned in Section 3.3 [62,88,91,92,125,127]. For example, Sokolov et al. compared P2VP/SiO_2 PNCs of the same φ_{NP} and molecular weight wherein all of the P2VP was grafted to the NP (a matrix-free PNC) or physically adsorbed to the NPs (a traditional PNC) [88]. Using BDS along with other techniques, they measured the α-relaxation [88] and β-relaxation [127] as a function of M_w. One of their main conclusions is that the degree of chain stretching in the interfacial layer critically affected the segmental dynamics. For low molecular weight systems, P2VP matrix-free and traditional PNCs exhibit similar interfacial dynamics while for intermediate M_w, where grafting induces chain stretching, the α-relaxation dynamics in matrix-free PNCs are slower than in traditional PNCs [88]. Other studies using BDS and NMR have also revealed slower α-relaxation dynamics for covalently bonded polymers to NPs as compared to physically adsorbed chains [91,125]. Note that secondary segmental relaxations (β-process) in the glassy state sometimes behave

differently. For example, in the aforementioned P2VP/SiO_2 matrix-free PNCs, secondary relaxations are faster relative to bulk while adsorbed chains in traditional PNCs are more bulk-like [127]. This observation and others [92,128] highlight the decoupling between α and β processes and the many parameters, such as chain stretching and local free volume, that affect the two differently. The use of polymer-grafted NPs adds variables to the already expansive parameter space for PNCs and more research investigating different regimes of R_{NP}, σ_{graft}, and graft M_w will help develop a thorough understanding of relaxations within the polymer brush in PNCs.

4. Intermediate polymer dynamics

4.1. Experimental and simulations methods

Intermediate polymer dynamics, also called Rouse dynamics in the melt [35], involve relaxations associated with chains of segments and are therefore slower than segmental dynamics (Section 3) and faster than the center-of-mass polymer diffusion (Section 5). The exact delineation between segmental dynamics and intermediate dynamics can sometimes be unclear, but we consider intermediate dynamics to be the collective motion of several segments. Experimentally, these intermediate dynamics are primarily measured using neutron scattering and rheology. MD simulations are insightful as well. Due to the limited experimental techniques and because these cooperative motions are often complicated to analyze, progress on understanding intermediate dynamics is comparatively slow, especially with respect to the dense parameter space presented by PNCs.

In unentangled polymer melts, the Rouse model describes the relaxation dynamics of chains with p-sized chains and can be extended to the full chain ($p \leq N$) [35]. When the degree of polymerization (N) exceeds the degree of polymerization between entanglements (N_e), the Rouse model describes relaxations within entanglement strands. However, larger scale dynamics ($p > N_e$) are considered confined to a tube formed by entanglement nodes, according to the Edwards tube model [35]. Clearly, intermediate dynamics are intimately tied to the entanglement network. In PNCs, the polymer entanglements are perturbed by the presence of NPs, so measurements of these intermediate dynamics can provide insight into entanglements in addition to the actual dynamics of sections of the chain.

Rheology is a dynamic mechanical measurement that measures the complex modulus (often shear, G' and G") as a function of frequency, usually with a polymer melt placed between parallel plates. For a neat polymer melt at shearing frequencies longer than the slowest characteristic relaxation of the material, the terminal flow regime is reached where $G' \sim \omega$ and $G'' \sim \omega^2$. At faster shearing frequencies, the frequency-dependent moduli changes with the dynamics in the sample, thus giving insight into intermediate dynamics. The addition of NPs often stiffens the polymer melt and usually introduces additional dynamic processes, such that extracting polymeric relaxation times from linear viscoelastic measurements of PNCs is difficult, especially at high NP concentrations [40] and for poorly dispersed systems [129]. In many cases, the rheological spectra can reflect NP-polymer interactions, dynamics of the NPs, *and* heterogenous dynamics of free and interfacial polymers. Deconvoluting these contributions can be arduous [130].

Inelastic neutron scattering methods, QENS and NSE, can access intermediate polymer dynamics more directly. For sufficiently flexible polymers with small Kuhn segments measured at $T \gg T_g$, QENS (Section 3.1) can measure Rouse dynamics. For example, QENS of polyethylene oxide (PEO, b = 0.6 nm) shows $\langle r^2 \rangle \sim t^{1/2}$, characteristic of Rouse dynamics [131]. However, QENS experiments on PS [37] and P2VP [55] (both with $b \sim 2$ nm) reveal various geometries of motion, but are generally incapable of accessing Rouse length- and time-scales. In NSE, the change in velocity of incident and scattered neutrons, which is related to the transfer of energy of the scattering event, can be precisely measured for a variety of q by monitoring neutron spin before and after the scattering event through Larmor precession [60]. NSE offers a wave vector range of $\sim 10^{-3}$ – nearly 1 $Å^{-1}$ (length scales of ~0.6–600 nm) and energy range of $\sim 10^{-1}$–10^{-6} meV (timescales of $\sim 10^{-11}$–10^{-6} s) and, thus, NSE is a powerful tool for probing intermediate polymer dynamics in PNCs. The normalized intermediate scattering functions, ISF or I(q,t), are directly obtained in NSE, and can be readily fit to system-specific functions including the Rouse model and reptation model. NSE requires specialized instrumental access available at global user facilities, necessitates collection times on the order of days per sample, and samples are often comprised of majority deuterated polymer.

Due to the complexity of dynamics of chains and chain segments, MD simulations are also useful to probe intermediate dynamics. In simulations, Rouse analysis can comprehensively extract the timescales associated with various sections of the chain (Rouse mode analysis) to further understand the relaxation mechanism. In addition, simulations access various parameters associated with the entanglement network via primitive path calculations that provide entanglement densities and visualizations of the Edwards tube in melts and PNCs [132–134]. Although the average tube diameter can be measured in NSE and the molecular weight between entanglements can be estimated from rheology, simulations provide unique insights about spatial heterogeneities and locations of the entanglements in PNCs.

4.2. Intermediate dynamics in PNCs

Measurements of the full rheological spectrum in PNCs usually explore up to three key relaxations: the relaxation time of a Rouse monomer (τ_0, on the order of b), the relaxation of the entanglement strand (τ_e for $N/N_e > 1$), and the terminal relaxation time (τ_t, on the order of R_g). The Rouse monomer relaxations, also called the elementary relaxations, measured by rheology are similar to measurements from BDS (as discussed in Section 3), while τ_e and τ_t relaxations are usually inaccessible to techniques discussed in Section 3.1. Several authors have made thorough rheological measurements to probe microscopic dynamic processes, but most suffer from gel-like PNC responses at high NP concentration [67,117,131,135–138], with some exceptions [108,139]. For example, by forming rheological master curves referenced to the T_g of PNCs comprised of PEG-grafted SiO_2 and PMMA, measurements of τ_0, τ_e, and τ_t revealed a monotonic increase in each relaxation time with the addition of NPs, indicating slowing across these length-scales [139]. More examples exist in a variety of PNC systems.

Rheology also provides measurements of viscosity that characterize how PNCs flow and provide insight related to intermediate and chain dynamics. The literature about viscosity in nanoparticle-filled polymers is expansive. Several parameters are known to affect the viscosity of PNCs, including NP-polymer interaction, polymer M_w, φ_{NP}, and NP size. Both increases [67,138,140–144] and decreases [139,140,145] in viscosity have been observed in PNCs, indicating complex and often competing effects of different variables. For large NPs in short polymers, the Einstein-Batchelor law [146] describes the increase in viscosity as a function of φ_{NP}:

$$\eta_{PNC}/\eta_{bulk} = 1 + 2.5\varphi_{NP} + 6.2\varphi_{NP}^2 \quad (3)$$

The viscosity increases above the prediction in Eq. (3) with strong NP-polymer attractions [142–144]. Decreased viscosity relative to bulk has been observed particularly in high M_w polymers filled with athermal or small NPs [139,140,145]. Kumar and coworkers proposed a “universal” behavior for viscosity in ather-

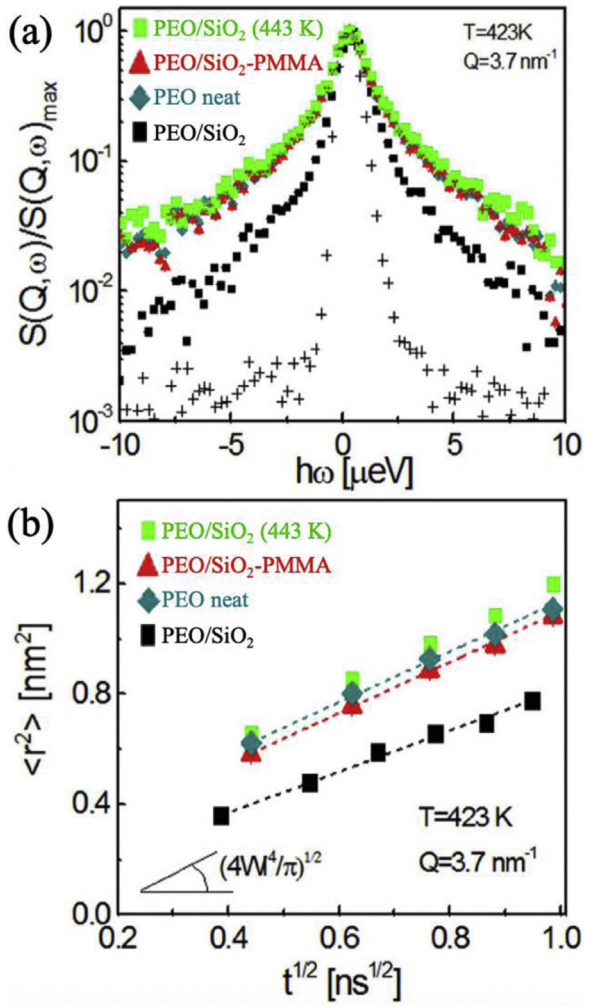

Fig. 8. Incoherent dynamic structure factor (top) and mean square displacement (bottom) of PEO in neat PEO (teal diamonds) and PEO-based PNCs composed of PMMA-coated SiO_2 (red triangles) and bare SiO_2 (black squares) at T = 423 K and bare SiO_2 in PEO at T = 443 K (green squares). All PNCs were filled with φ_{NP} = 17.6% (core only) [141]. Copyright 2016. (For interpretation of the references to color in this figure legend, the reader is referred to the web version of this article.)
Reproduced with permission from Nature Springer Ltd.

mal and attractive PNCs by considering only polymer M_w and NP size [147]. While this treatment captures many experimental studies and serves as a zeroth-order description of viscosity deviations from bulk, it fails to capture some experimental results and remains to be fully tested with a more expansive set of materials and parameters. These results (as well as other rheological measurements) imply that mechanical measurements and viscosity are complex functions of several variables and dynamic processes that synergistically affect stress relaxation behavior.

We next discuss more direct measurements of intermediate dynamics through neutron scattering. For example, PEO-based PNCs with different NP-polymer interactions were probed using QENS and NSE. The PNCs contained either bare SiO_2 NPs or SiO_2 NPs coated with polymethyl methacrylate (PMMA) and dispersed in PEO [141]. Interestingly, the QENS broadening for PEO-SiO_2/PMMA matches bulk PEO, while the QENS broadening is narrower for PEO-SiO_2/bare systems, indicating slower PEO intermediate dynamics (Fig. 8) [141]. In both sets of PNCs, after the Fourier transformation of S(q,ω) and using the relation $S(q,t) = \exp\left[-q^2/6\left\langle r^2(t)\right\rangle\right]$, Rouse scaling is observed where $\left\langle r^2(t)\right\rangle \sim t^{1/2}$ [141]. The authors attribute the decreased $\left\langle r^2(t)\right\rangle$ and reduced Rouse parameter (Wl^4) to PEO adsorption to SiO_2, because this analysis inherently assumes a homogeneous model (Fig. 3). Complimentary NSE measurements on these PNCs revealed similar dynamics at short times. At long times, disentanglement was observed in the PEO-based PNCs with glassy PMMA-coated SiO_2, while the entanglement network was largely unperturbed in the other PNCs studied [141]. These neutron measurements provided a microscopic view of segmental and intermediate dynamics in PNCs with different interactions, although the PMMA-mediated NPs introduce additional interfacial complexities that remain largely unknown.

In another set of measurements on low M_w PEO/SiO_2 PNCs, the interfacial interactions were altered by the polymer end group [77]. Although Rouse dynamics were slowed in these PNCs relative to neat polymer, OH-terminated chains exhibited a larger perturbation than CH_3-terminated chains, showing that attractive interactions even at the chain ends slow Rouse dynamics in PNCs [77]. In a largely non-attractive set of PNCs, Richter and coworkers studied dynamics of PEP segments and chains in PNCs with SiO_2 NPs [148,149]. In these PNCs, the Rouse dynamics were unperturbed relative to bulk, even at high φ_{NP} (~60 vol%) and the population of dynamics within the PNCs remained bulk like (unlike the heterogeneous dynamics discussed in Section 3.2). Using these cases as examples, the NP-polymer interactions certainly affect intermediate dynamics and in many cases, insights from segmental dynamics can be extended to Rouse dynamics for $p < N_e$.

The intermediate dynamics of polymers grafted to NPs has also been measured in a few contributions but much remains unknown [92,128,150]. In general, confined dynamics are observed as the grafted-chains restrict Rouse motion of adjacent chains and the presences and magnitude of this effect depends strongly on grafted M_w, σ, and R_{NP} [27,33]. In matrix-free PNCs, polyisoprene segmental dynamics were found to be relatively unperturbed until large enough Rouse length-scales where grafted chains interacted with adjacent grafts and were slowed relative to bulk [92]. Upon the addition of matrix chains forming a traditional PNC, the topological constraint was reduced [92]. In solutions of SiO_2 NPs with selective isotopically labelled polymer grafts studied by NSE, slow Zimm dynamics (akin to Rouse dynamics in the melt) were observed near the polymer interface but faster dynamics were observed far from the NP surface [150]. Understanding the heterogenous dynamics within the polymer brush on NPs in the melt and documenting the dependence on various PNC and NP variables is critical to understanding PNCs with grafted NPs.

The effect of NP size has also been measured on Rouse-like time scales. Using NSE to study PEO-based PNCs with PEG-functionalized 3-nm and 20-nm gold NPs (an athermal system), Faraone and coworkers showed Rouse dynamics were comparable to neat PEO and largely unaffected by NP size [131]. Whether this NP size-independent observation holds for attractive interactions or higher NP concentrations remains to be explored. In a combined QENS and NSE study, poly(vinyl methyl ether) (PVME) was filled with glassy polystyrene-based NPs of different M_w [151]. The Rouse dynamics of PVME in these PNCs were slower than bulk and the slowing was independent of PS architecture (linear or star) or M_w according to QENS [151]. NSE measurements also showed slower collective PVME dynamics in the PNCs and, interestingly, revealed a difference between the PS NPs from linear and star polymers. The authors attribute this effect to geometric confinement that was only apparent at the longer length-scales accessible to NSE [151].

As mentioned before, experimental progress on understanding dynamics in this intermediate regime is comparatively slow and measurements are significantly scarcer as compared to other dynamic processes, especially with regard to the dense parameter space inherent to PNCs. Using MD simulations, the effect of NP concentration [152], NP size [153–155], and NP-polymer

interaction [153,156] on Rouse dynamics was probed. At low φ_{NP}, coarse-grained MD simulations show the local Rouse dynamics are largely unperturbed although the disentanglement time gets faster [152]. At high φ_{NP} (at least 31 vol%), NPs become confining to the Rouse motion and disentanglement time and local relaxations begin to slow down [152]. In a thorough study of Rouse relaxation in athermal PNCs, Rouse relaxations were faster in PNCs with small NPs ($R_{NP} < d_{tube}$) and largely unaffected in PNCs with larger NPs [155]. In general, it is reported that Rouse dynamics over different length-scales are more perturbed in PNCs with favorable NP-polymer interactions [153,156]. For entangled chains ($N > N_e$), the intermediate dynamics follow expectations from changes in the entanglement network, as discussed in Section 4.3.

4.3. Entanglement network in PNCs

Entangled polymers at intermediate timescales are confined by the entanglement network in the polymer melt. As a result, at timescales beyond Rouse relaxations, a long-time plateau is observed in S(q,t) from NSE and an entanglement plateau is observed in rheology as segments cannot relax beyond topological entanglements. This entanglement network is described by a confining tube in the Edwards model. Given enough time, polymer chains will escape their confining tube or the entanglement network will relax, leading to chain diffusion discussed in Section 5. However, measurements of intermediate dynamics in polymer melts gives insights into the entanglement network.

To understand how spherical NPs perturb the entanglement network, Richter and coworkers measured NSE on poly(ethylene-alt-propylene) (PEP) based PNCs as a function of hydrophobic-SiO_2 NP concentration and fit S(q,t) at long times to extract the tube diameter, Fig. 9. [149,157]. As φ_{NP} increases from bulk (black) to 60% (purple), polymer chains become more confined and the apparent tube diameter, d_{app}, decreases [149]. Importantly, this PNC system exhibits reasonable NP dispersion, unperturbed local segmental dynamics and Gaussian polymer conformations as measured by TEM, NSE, and small angle neutron scattering (SANS), respectively [149,157]. To understand the decrease in the d_{app}, the authors define "particle entanglements" to describe the impact of geometric confinement imposed by the NPs (d_{geo}) by estimating the void distribution function. With knowledge of d_{app} and d_{geo}, the tube diameter associated with only the polymer matrix (d_{tube}) can be evaluated by assuming Gaussian statistics and is found to increase significantly with φ_{NP}, Fig. 9 [149]. This result, that the addition of NPs effectively decreases the tube diameter (adding effective entanglements) through geometric constraints and increase the tube diameter (removing polymer entanglements) of the polymer network, is also observed in MD simulations [152] and first-principles theory [158]. In MD simulations, below a critical volume fraction ($\varphi_c = 31$ v%) the chain dynamics are controlled by polymer entanglements, while above φ_c the geometric confinement or NP entanglements dominate the intermediate polymer dynamics [152]. A reduction in d_{app} was reproduced theoretically using mixtures of rods and spheres and the magnitude of the reduction was found to depend on only the volume fraction of NPs and the dimensions of the rods and spheres [158]. The convergence of this theory, simulations, and experiments establishes how spherical NPs perturb the entanglement network in model PNCs.

It is well known that small molecular additives (such as a solvent) or a low-M_w polymer act to disentangle high M_w polymer and increase d_{tube}, so it is reasonable to expect small NPs may have similar effects. Faraone and coworkers show exactly this: the addition of 20-nm diameter athermal Au NPs to PEO at $\varphi_{NP} = 20$ vol% does not measurably perturb the apparent tube diameter (as measured by NSE), but 3-nm diameter athermal Au NPs increase the tube diameter by ~25% at the same φ_{NP} [131]. This concept of tube dilation has been observed and discussed in other PNC systems as well [109,145,159].

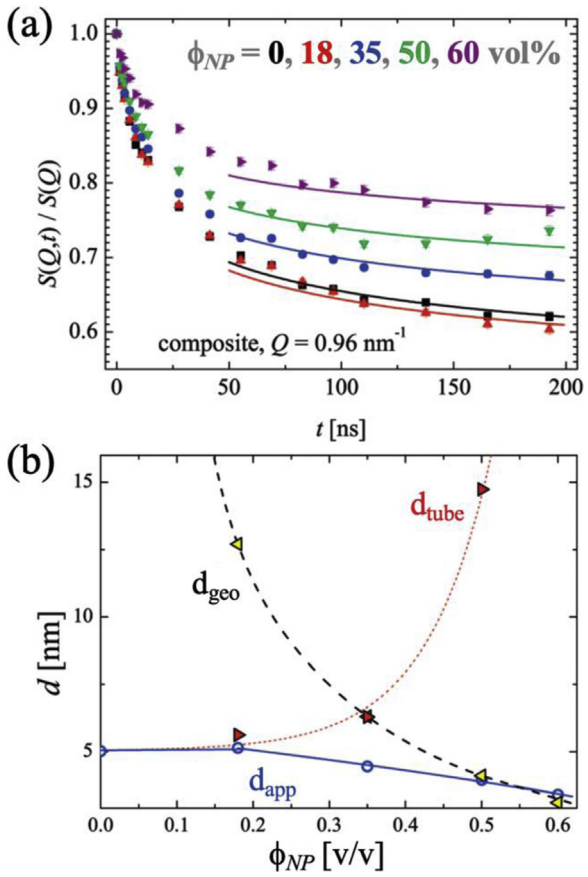

Fig. 9. (a) Normalized dynamic structure factor from NSE of PEP for a variety of NP concentrations ($\varphi_{NP} = 0$, 0.18, 0.35, 0.5, and 0.6 from black squares to purple tilted-triangles and $2R_{NP} = 17$ nm). (b) Separation of apparent tube diameter, d_{app}, measured in (top) and contributions of polymer entanglements (d_{tube}) and geometric NP-induced entanglements (d_{geo}) [149]. Copyright 2011. (For interpretation of the references to color in this figure legend, the reader is referred to the web version of this article.)

Adapted with permission from the American Chemical Society.

MD simulations also provide valuable information about the entanglement network in PNCs [152,153,160–165]. For example, PNCs with athermal NPs and $R_g \gg R_{NP}$ exhibit disentanglement ($N_{e,PNC} > N_{e,bulk}$) and more specifically, a depletion of entanglements near the NP [165]. Moreover, the NPs often contribute to the primitive path indicating that NPs can act as topological constraints akin to entanglements [165]. These observations agree with aforementioned NSE results. In another simulation, the entanglement tube diameter increased as a function of NP concentration, demonstrating disentanglement, and this increase was larger for smaller NPs and stronger NP-polymer attractions [162,166]. It is important to note that in simulations, the entanglement network is defined by the primitive network but in experiments, it is usually defined by polymer dynamics or stress relaxation, so NPs may contribute differently.

5. Polymer chain diffusion

5.1. Experimental and simulation methods

As described in Section 4.1, rheology and NSE provide insights to chain-scale diffusion in certain systems and experimental conditions. For example, without NP percolation or significant mechanical stiffening, the terminal relaxation behavior in rheolog-

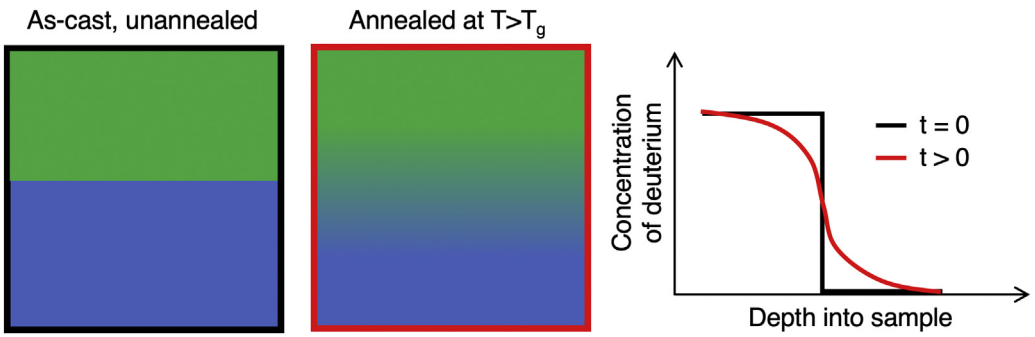

Fig. 10. General schematic of diffusion experiment using a mutual diffusion sample configuration.

ical spectra provides a measurement of the largest relaxation time (τ_t) associated with the chain, which can be used to estimate the polymer diffusion coefficient. In addition, the diffusion of unentangled chains can be measured by NSE and BDS at $T \gg T_g$. While NSE measurements of ISF often plateau at long times due to the confined relaxations in the entanglement mesh, full decorrelation can be observed in unentangled polymer chains [148]. In addition, for polymers with a permanent dipole along the backbone (such as PPG), BDS can measure the so-called normal mode relaxation time, which represents full chain relaxation [167]. Specialized NMR techniques can also be used to measure the diffusion coefficient in PNCs, but this measurement is generally less common [168].

The most common way to measure chain-scale center-of-mass diffusion in PNCs is through depth profiling, Fig. 10. Typically, a bilayer film of deuterated and protonated polymer is assembled and annealed at $T>T_g$. While the interface is initially sharp, as chains diffuse they interpenetrate and the interface broadens. By measuring the depth profile of the deuterated chains in the protonated matrix and knowing the annealing time, the interdiffusion rate or diffusion coefficient can be determined. Deuterium depth profiles are most commonly measured by elastic recoil detection (ERD), secondary ion mass spectroscopy (SIMS) or neutron reflectivity (NR).

Elastic recoil detection (ERD) offers a relatively large penetration depth and can characterize the depth profile up to nearly 800 nm with less than or approximately 80 nm resolution. [169] In ERD, ^{4}He ions of known energy are accelerated towards the sample at a glancing angle and light elements such as ^{1}H and ^{2}D are forward recoiled toward the detector where their energy is measured. With knowledge of the beam parameters and atomic composition of the sample, the difference in measured and incident energy can be related to the depth of the collision event. These samples typically consist of a thin deuterated polymer film (<50 nm) on a protonated polymer film (>10 μm), namely a tracer configuration. Following Fig. 10 (but where the green tracer polymer is much thinner than the blue matrix) these diffusion couples are annealed at $T>T_g$ for a variety of annealing times, then cooled below T_g. The depth profile of the deuterated species is measured ex situ and a diffusion coefficient is extracted by fitting the deuterated depth profile with a solution to Fick's second law assuming a finite source in a semi-infinite medium [169,170].

In SIMS, an incident ion beam rasters over the sample surface to sputter ions and atoms from the sample. To measure the concentration of different elements, the charged species are detected by a mass spectrometer tuned to the appropriate elemental mass [171]. Typical samples are nearly symmetric bilayer films as depicted in Fig. 10 with total thicknesses on the order of 300 nm. The penetration depth in SIMS is defined by the raster duration, intensities, and geometries and the maximum practical depth is on the order of several hundred nanometers. The depth resolution of dynamics SIMS and time-of-flight SIMS is typically on the order of 10 nm [172].

Neutron reflectivity (NR) is a depth profiling technique for thin films where highly collimated neutrons are incident on the sample surface and the reflected intensity is measured as a function of incident angle [173]. Since neutrons are sensitive to differences in atomic nuclei, especially isotopes ^{1}H and ^{2}D, the reflectivity profile can be fit to reveal the concentration depth profile. NR offers a depth resolution and depth penetration on the order of ~1 nm and ~200 nm, respectively [173]. Samples for NR are usually comprised of a bilayer of deuterated and protonated films, each usually ~100 nm or less. Unlike ERD or SIMS that rely on ex situ annealing, NR experiments can be either ex situ or in situ. To fit NR data for interdiffusion, the diffusion profile is often assumed to follow an error function between pure ^{1}H and ^{2}D phases and the interfacial width is extracted as a function of time. An observed increase in interfacial width with $t^{1/2}$ is indicative of polymer diffusion, although sometimes NR length scales are too small to reach this regime.

Diffusive dynamics can also be studied through molecular dynamics, Monte Carlo, and various other methods, as recently summarized for melts and PNCs [32]. Molecular dynamics simulations are most common using coarse-graining methods to alleviate the computational expense of long simulation times. The Kremer-Grest model introduced in Section 3.1 is often used, but imposes a practical limit of lightly entangled chains ($N/N_e < 10$). Monte Carlo simulations are commonly used to model diffusion of entangled chains [136,154,174–176]. Other models including dissipative particle dynamics and slip-spring simulations [32] and force-based theoretical predictions [177] are less common but have been applied.

5.2. Polymer diffusion in the presence of spherical nanoparticles

The inclusion of NPs in a polymer matrix often impedes chain-scale polymer center-of-mass diffusion. This effect can be anticipated because polymer chains need to diffuse around impenetrable NPs, thus causing a longer diffusion trajectory. One may expect this to be confounded by other influences including altered polymer conformations, unique interactions, and changes to smaller-scale dynamics or the entanglement network, all of which may have non-trivial influences on polymer diffusion.

We start this discussion with the simple case of entangled polymer diffusion in the presence of athermal NPs. Composto and coworkers used ERD to measure dPS tracer diffusion (M_w = 49–530 kg/mol) into PS-based PNCs [178] with well-dispersed phenyl-functionalized 28-nm SiO_2 NPs at φ_{NP} = 0–50 vol% [170]. Polymer tracer diffusion was slowed as a function of φ_{NP} to a degree larger than expected from excluded volume and tortuosity, as predicted by the Maxwell model [179]. These results were in line with the entropic barrier model [174,175]. Furthermore, a master curve was developed by plotting the diffusion coefficient relative to the diffusion coefficient of neat polymer (D/D_0) as a func-

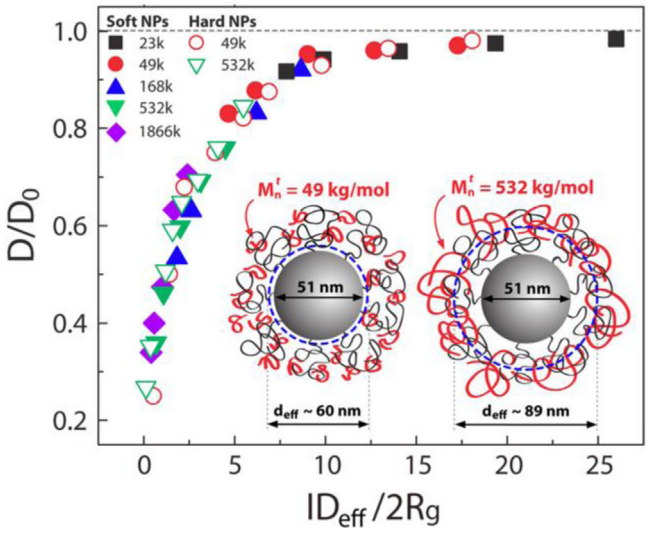

Fig. 11. Master curve developed for a variety of PS-based PNC systems showing collapse of the tracer diffusion coefficient normalized to bulk as a function of the effective interparticle distance relative to the tracer polymer chain size. Filled and open symbols refer to grafted and bare NPs, respectively [182]. Copyright 2013.
Reproduced with permission from the American Chemical Society.

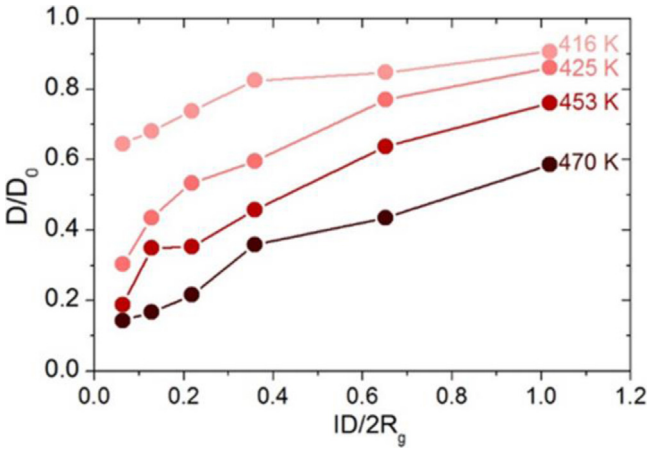

Fig. 12. Temperature dependence of polymer diffusion showing more perturbed diffusion at higher temperatures. Measurements are for 532 kg/mol dPS diffusion into PS/SiO_2 PNCs (φ_{NP} = 0–50 vol%, $2R_{NP}$ = 28.5 nm, $T_g^{PS} \sim 375$ K) [188]. Copyright 2016.
Adapted with permission from the American Chemical Society.

tion of $ID/2R_g$, or interparticle separation distance (ID) relative to the size of the deuterated polymer ($2R_g$) [170].

In later publications, a similar collapse was observed for ERD measurements of tracer diffusion in various PNCs to probe the influence of NP size [180,181], NP polydispersity [181], interfacial interactions [180], and interface softness using grafted NPs [182,183]. The effective interparticle distance (ID_{eff}) is used to account for the polydispersity of NPs and the volume accessible to the tracer molecule in the presence of densely grafted NPs, Fig. 11 [181,182]. At the limits, D is reduced nearly an order of magnitude in strongly confined PNCs ($ID_{eff}/2R_g < 1$) and the reduction in tracer diffusion extends to weakly confining PNCs, where bulk diffusion is only recovered at $ID_{eff}/2R_g \sim 20$. To compare with these experiments, Meth et al. developed an analytical method that treats polymers diffusing through nanocomposites as spheres diffusing through cylinders (mimicking the network of free space in the PNC) [184]. This model quantitatively agrees with data in Fig. 11 at $ID/2R_g > 5$ and underestimates D/D_0 at $ID/2Rg < 5$, likely because the model does not account for perturbed conformations or entropic penalties.

Measurements of chain diffusion from an attractive interface [185–187] and segmental dynamics near attractive NPs (Section 3.2) imply that attractive interactions may impact chain-scale dynamics. Composto and coworkers compared PS/SiO_2-Ph (athermal interactions) and PMMA/SiO_2 (attractive interactions) and observed that tracer diffusion through these PNCs are independent of interfacial interactions [180]. This result suggests that tracer polymer molecules can diffuse within the bound layer in PMMA/SiO_2 and the increased friction at the NP-polymer interface is either similar to PS/SiO_2-Ph or insignificant.

The collapse presented in Fig. 11, as measured by ERD, is at a fixed T-T_g with large M_w polymer for the protonated matrix. Although a qualitatively similar dependence on $ID/2R_g$ exists over a range of temperatures, the normalized tracer diffusion is more perturbed from bulk at higher temperatures (Fig. 12) [188]. This difference was reconciled by entropic arguments, where the entropic barrier extracted from temperature-dependent measurements scaled with $ID^{-0.5}$, consistent with an entropic perturbation imposed by the NPs. This result highlights that the convenient and successful scaling of $ID/2R_g$ omits the temperature dependence of the physics governing tracer diffusion through PNCs. Also note that Fig. 11 applies to PNCs wherein the spherical NPs are immobile on the timescale of polymer diffusion. ERD studies of very small, attractive NPs (~2 nm OAPS) in P2VP found polymer diffusion to be more dependent on φ_{NP} than measurements in PS/SiO_2 PNCs at the same temperature [109]. By comparing D/D_0 with $\tau_\alpha/\tau_{\alpha,0}$ and measuring NP diffusion, a friction-dominated mechanism was proposed for the P2VP/OAPS system with mobile NPs [109]. In summary, the master curve in Fig. 11 is appropriate for tracer diffusion in PNCs with immobile spherical NPs under isothermal conditions.

In addition to the ERD measurements of tracer diffusion, other techniques have been applied to the problem of polymer diffusion in PNCs. Early measurements of pulsed-gradient spin-echo NMR on entangled PE diffusion in PE/ZnO PNCs (non-attractive) showed bulk-like diffusion in PNCs of varying M_w, NP concentration, and NP size [189]. This observation may result from low φ_{NP} and poor NP dispersion, among other factors. In a study using in-situ neutron reflectivity, entangled PS diffusion in all-polymer athermal PNCs comprised of PS and soft crosslinked-PS NPs were measured [190,191]. In these measurements, the relative size of NPs and polymers lead to enhanced or suppressed diffusion resulting from the competing effects of constraint release or disentanglement and added topological barriers, respectively [191]. To be specific, for small PS NPs in large M_w PS, $D/D_0 > 1$ was observed and attributed to increased constraint release akin to a diluent. Conversely, for large NPs in low M_w polymer, polymer diffusion was slowed apparently by the presence of barriers, qualitatively similar to ERD measurements with immobile NPs, although NP softness may contribute [190,191]. In another contribution, the segmental dynamics and translational diffusion of unentangled PEP chains in the presence of SiO_2 NPs was measured via NSE which showed slow chain diffusion beyond expected solely from geometric confinement, which is consistent with increased friction or entropic effects associated with confined diffusion [148].

As recently reviewed [32], computer simulations have been broadly applied to polymer diffusion in PNCs to investigate the extensive parameter space such as NP-polymer interactions [124,153,163,192], NP size [136,193,194], polymer M_w [195], and other factors [176,194]. Early MD simulations by Kumar et al. showed polymer diffusion in the presence of attractive NPs slowed monotonically with increasing φ_{NP} [192]. In contrast, PNCs with repulsive NPs exhibited diffusion faster than bulk ($D/D_0 > 1$) at $\varphi_{NP} < 8$ vol% and slower at higher φ_{NP}, implying that diffusion at

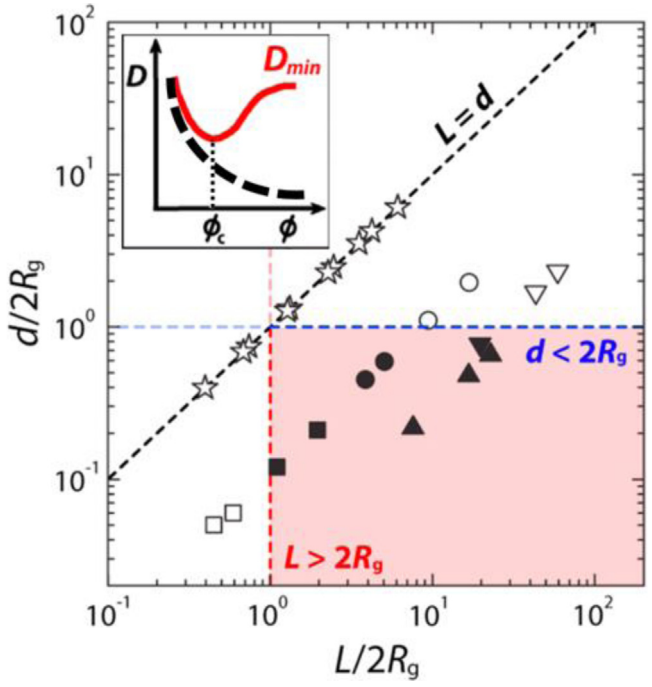

Fig. 13. Diagram representing the effect of NP diameter and length relative to polymer R_g on observations of monotonic (open symbols) or non-monotonic (closed symbols) dependence of normalized tracer diffusion coefficient as a function of NP concentration, as schematically shown in the inset. Data is compiled from PNCs containing spherical SiO_2 (star symbols), CNTs (triangle symbols), and nanorods (square and circle symbols) [201]. Copyright 2014.
Adapted with permission from the American Chemical Society.

low φ_{NP} results from interfacial perturbations [192]. Other simulations have observed $D/D_0 < 1$ in repulsive and attractive PNC systems, and observed behavior that deviated from experimental results presented in Fig. 11 [194,195]. For example, while a qualitatively similar trend with $ID/2R_g$ was recently observed using a dynamic Monte Carlo technique, larger NPs perturb diffusion more strongly than smaller NPs, even at the same ID [194].

5.3. Polymer diffusion in the presence of non-spherical nanoparticles

Understanding the impact of anisotropic NPs on polymer translational diffusion requires consideration of the multiple length-scales associated with the non-spherical NPs. For example, whereas spherical NPs have one characteristic size (R_{NP}), cylindrically-shaped NPs have two relevant length scales (R_{NP} and L). Fig. 13 shows that geometric considerations of the NP length (L) and diameter ($d = 2R_{NP}$) relative to R_g distinguish monotonic (open symbols) and nonmonotonic (closed symbols) dependencies of polymer normalized tracer diffusion coefficient as a function of φ_{NP}. For highly anisotropic NPs with $2R_{NP} < 2R_g < L$ (red region in Fig. 13), polymer diffusion slows relative to bulk at small φ_{NP} and slowly recovers at φ_{NP} larger than the critical concentration ($\varphi_{NP,c}$) [196–201]. For PNCs with spherical NPs in Section 5.2 or less anisotropic NPs, the polymer diffusion coefficient decreases monotonically with φ_{NP} [170,180,182,197,200,201]. These different dependencies of D/D_0 vs φ_{NP} are shown schematically in the inset of Fig. 13. This comparison highlights that the perturbation to polymer dynamics changes considerably when only one dimension of the NP is smaller than the chain size.

The non-monotonic decrease in D with φ_{NP} was first observed in PS-based PNCs comprised of highly anisotropic single-walled carbon nanotube (CNT) bundles using ERD [196–198]. The D/D_0 reaches a minimum value at $\varphi_{NP,c}$, which correlates with the mechanical percolation threshold as determined by DMA. Furthermore, $\varphi_{NP,c}$ was found to depend on the PS matrix M_w and not dPS tracer M_w [196] or temperature [198], but both M_w and T affected the minimum value of D/D_0. A trap model was simultaneously developed to test the hypothesis that diffusion along CNTs is faster than diffusion perpendicular to CNTs [196]. This model qualitatively captures the decrease in $\varphi_{NP,c}$ with increasing matrix M_w and decrease in the minimum value of D/D_0 with decreasing tracer M_w, suggesting that anisotropic diffusion could be the origin of a minimum in D/D_0 as a function of φ_{NP} [196]. Other simulations further developed these results [161,163,202]. Using a variety of tracer M_w with multi-walled CNTs [197,198], long and short TiO_2 NRs [200,201], and spherical NPs in chain-like aggregates [199], it was determined that when $D_{NP} \ll D_{polymer}$, the general criteria for observation of a minimum D/D_0 (i.e. anisotropic diffusion) is $2R_{NP} < 2R_g < L$, Fig. 13.

When NPs are small relative to the entanglement network ($2R_{NP} < d_{tube}$), NP diffusion can be fast compared to the polymer diffusion and therefore can be considered mobile during polymer relaxations [203]. By using φ_{NP} and matrix M_w to control the nanorod mobility, the dPS tracer diffusion coefficient into PS/TiO_2 ($2R_{NP} < L < 2R_g$) nanorod-based PNCs with mobile ($D_{NP} > D_{chain}$) and immobile ($D_{NP} < D_{chain}$) NPs was measured [200]. While polymer diffusion in the PNC was consistently slower than bulk diffusion ($D/D_0 < 1$), faster polymer diffusion was observed in PNCs with mobile NPs than immobile NPs at the same φ_{NP} [200]. This enhanced polymer diffusion in the presence of mobile anisotropic NPs was captured by a numerical slip-spring model which provides a mechanistic understanding. The model includes fixed topological constraints (representing those from the PS matrix and immobile NRs) and additional constraints that have a finite release time (representing those from mobile NRs) [200]. The inclusion of constraints with a finite release time leads to faster polymer diffusion as compared to when all constraints are fixed. These results, along with those with mobile spherical NPs [109], clearly demonstrate the importance of NP mobility in understanding the polymer diffusion dynamics.

Experiments probing polymer diffusion through PNCs with NPs of other geometries, including plates/platelets, non-linear NRs, and self-assembled structures, are quite limited. In one study, polymer diffusion was measured using SIMS in dPMMA and dPS into PNCs containing 5 vol% montmorillonite clay platelets [22]. The diffusion of dPMMA in these clay PNCs was 3x slower than bulk while the diffusion of dPS was unperturbed from bulk, a difference that was attributed to preferential adsorption of PMMA chains but these results may be confounded by poor dispersion and surface aggregation. Future studies of polymer diffusion in PNCs with well-dispersed planar NPs would further develop Fig. 13.

5.4. Exchange dynamics from the NP interface

Analogous to the separation of segmental dynamics in the bound layer from those of free chains (Section 3.2 and Fig. 3), a recent experimental direction that has emerged is measuring the desorption, or exchange dynamics of bound chains in the melt state. Exchange dynamics from a flat substrate have been studied by depth profiling techniques such as SIMS, ERD, and NR [185–187,204,205]. Generally, these studies reveal polymer diffusion slows near a solid interface [204,205], depends on the polymer-substrate interaction [187,205], and the effect is spatially long-lasting (in that slow polymer diffusion is observed at distances well beyond R_g from the interface) [186]. However, exploring polymer exchange dynamics in PNCs is considerably more challenging because experimentally distinguishing bound polymer and free

polymer is difficult. Unfortunately, MD simulations are typically too slow to study polymer desorption.

Recently, polymer exchange has been probed in P2VP/SiO_2 PNCs using two different experimental approaches: SANS [206] and ERD [207]. For SANS, dP2VP/SiO_2 PNCs were successively solvent washed to remove free polymer and the dP2VP-coated SiO_2 NPs were redispersed in protonated P2VP. These PNCs with deuterated bound layers were then annealed at two temperatures for various times, measured using SANS, and analyzed by assuming a core-shell model where the shell is the dP2VP bound layer [206]. The dP2VP shell thickness decreased from ~3 nm to ~0.6 nm when annealing at T_g+75 °C, but remained largely unchanged after annealing at T_g+50 °C, indicating a strong temperature-dependent process [206]. Using ERD measurements on P2VP/SiO_2 PNCs, the fraction of bound chains was measured in the melt state after conventional PNC fabrication procedures by spatially separating free polymer from bound polymer as a function of annealing time, annealing temperature, and M_w. First, measurements at relatively short annealing conditions isolate NP-bound polymer from free polymer, and a bound layer of ~R_g was observed, as expected from other measurements [208–210]. Upon further annealing, polymer desorption was observed as the fraction of chains originally bound to the NPs decreased, and some polymer remained adsorbed after all annealing conditions studied [206]. In fact, the kinetics of desorption were slower for lower temperatures and higher M_w, and this effect correlates with the polymer chain relaxation time, albeit over a relatively narrow window of M_w and temperature in this study. Despite differences in sample preparation and measurements, these two studies are in qualitative agreement in that polymer desorption is much slower than bulk polymer dynamics, some chains remain bound for experimentally inaccessible time-scales (>10^6 τ_t), and the desorption kinetics depend strongly on temperature.

Much remains unknown about the desorption and exchange process of bound polymers in PNCs. First and foremost, the dense parameter space in PNCs remains largely untested, particularly NP size and NP-polymer interactions. In addition, ERD and SANS studies of P2VP/SiO_2 showed that some chains remained adsorbed for experimentally accessible time-scales [206,207]. It remains unclear how this observation and others depends on the material system or if PNCs with weaker interactions will also show "permanently" bound polymer. In addition, the interfacial conformations and evolution of conformations during annealing are unexplored and will require the development of techniques beyond those mentioned here. Finally, a mechanistic description of the desorption and exchange of different populations of chains (tightly bound vs lightly bound) remains elusive and may require considerable experimental and simulation efforts. This is a fruitful direction of research, even though the desorption process is expected to be very complicated and depend strongly on various experimental and PNC parameters.

6. Nanoparticle diffusion in polymer melts

6.1. Theoretical background

The Stokes-Einstein (SE) relationship describes the diffusion of spherical particles (D_{SE}) through a continuous medium as a competition between driving forces from thermal fluctuations and viscous drag forces of the medium:

$$D_{SE} = \frac{kT}{f\pi\eta R_p} \quad (4)$$

where η is the viscosity of the medium, R_p is the particle radius, kT is the thermal energy term, and f is either 4 or 6 for slip or non-slip conditions at the interface, respectively [38]. Eq. (4) assumes the characteristic particle size exceeds the largest characteristic length scale of the medium, i.e. R_g in a polymer melt. To apply The SE model to nanoparticle diffusion in polymer melts, the zero-shear viscosity (η_0) and core NP size (R_{NP}) are often used for η and R_p, respectively.

In polymer melts (i.e. in PNCs), deviations from SE behavior are expected [38]. Several theories have been developed to describe the diffusion of dilute nanoparticles in polymer melts, including by De Gennes [38], Rubinstein [211,212], Schweizer [213–217], and others [218,219]. Early work by De Gennes an coworkers qualitatively predicted that small NPs diffuse faster than $D_{SE}(\eta_0, R_{NP})$, because NPs sample a length-scale dependent friction dictated by Rouse relaxations when $2R_{NP}$~d_{tube} or by monomeric relaxations when $2R_{NP}$~b, both of which decrease the drag forces [38]. This concept was further developed quantitatively for repulsive NPs of various sizes in entangled and unentangled polymer melts, as discussed further in Section 6.3 [211–213,215,216,218]. More recently, theory was developed that begins to tackle the case of attractive NPs in Section 6.4 [214].

6.2. Experimental and simulation methods

Rutherford Backscattering spectrometry (RBS) is an ion beam method analogous to ERD, which was introduced in Section 5.1 and can be used to measure NP diffusion. RBS is used to measure the depth profile of elements heavier than H or D. In RBS, He ions are incident to the sample, typically in normal geometry, and are backscattered to a detector to measure the particle energy. The loss in energy is related to the incident energy, the kinematic factor of the collision (which depends on colliding particles), and the energy loss through the sample, and can provide a direct measure of the composition as a function of depth. RBS offers a depth resolution of <100 nm and a depth penetration of ~1 μm [169]. To measure NP diffusion using RBS bilayer samples typically comprise a ~150 nm layer of PNCs with low NP concentration on a bulk matrix of the same polymer. As samples are annealed at T>T_g, the NP depth profile is monitored by tracking the relevant elements (e.g. Si for SiO_2 NPs). Similar to ERD, the measured depth profiles are fit with a solution to Fick's second law and a diffusion coefficient is extracted. RBS requires access to an ion beam facility and data reduction and interpretation can be difficult, but it can survey a wide array of R_{NP}, η, M_w, annealing conditions, and can be applied to many different material systems.

Dynamic scattering measurements can also be used to measure the diffusion of NPs in a polymer melt, including X-ray photon correlation spectroscopy (XPCS) and dynamics light scattering (DLS). Fundamentally, both techniques are similar in that they measure the temporal fluctuations of the speckle patterns produced by coherent light scattering from dilute NPs in a polymer medium. They differ, however, in the specifics of the measurement, details of the instrumentation, and the length and time scales that they probe. XPCS uses a high-brilliance coherent X-ray source to measure the decorrelation in the spatial distribution of electron density in the sample as a function of q. Generally, XPCS offers a q range of 0.002 $Å^{-1}$ < q < 0.07 $Å^{-1}$ (spanning length scales of ~5–250 nm) and a dynamic range of ~500 μs to ~10^3 s. Analysis of the intensity time-autocorrelation functions, which are related to the ISF, uses a stretched exponential to reveal the relaxation time of the system. Plotting the extracted relaxation time vs q reveals the geometry of the motion where τ~q^{-2} is purely diffusive motion. In contrast, DLS uses a longer wavelength light, the scattering comes from differences in index of refraction, and typically only one q value is measured. Both methods can probe NP motion in PNCs with dilute (φ_{NP} < ~1 vol%) or concentrated PNCs and provide access to unique length- and timescales. As with RBS, these provide an ensemble

average of the NP dynamics and may be difficult to interpret or separate different dynamic processes in PNC systems.

More specialized measurements of NP dynamics exist as well. For example, a modified fluctuation correlation spectroscopy (FCS) method has been applied to melts and solutions [220,221]. Here, a laser is rastered over the polymer melt with a dilute NP concentration until an increase in the photon count is observed as indication of the presence of a NP. After the NP is placed in the focal volume of the laser beam, the photon counts are continuously recorded until the value reaches the background count, indicating that the NP diffused out of the focal volume. The diffusion coefficient is obtained by the decay time of the photon counts (extracted with a stretched exponential) and the size of the focused laser beam. Single particle tracking (SPT) has been applied to polymer solutions and gels [222–224] and, more recently, to polymer melts with NPs [225]. SPT uses either florescent or photon-emitting NPs (such as quantum dots) to precisely measure the center-of-mass position of individual NPs as a function of time [224]. From this measurement, van Hove distributions and mean-squared displacement (MSD) curves are constructed to analyze the distribution of dynamics, isolate different populations, and calculate the ensemble average. Although the requirements on the PNC system are somewhat stringent in that the NPs must emit light and the polymeric matrix must have a low T_g (since it is difficult to heat the sample), SPT can uniquely sample the motion of each individual NP and provide unique insight into the population of dynamics.

Finally, coarse-grained MD simulations can also probe NP motion in polymer melts. The NPs can either be constructed as a single bead with larger size and mass or a collection of smaller beads. The latter option reduces artificial crystallization and dense packing at the NP-polymer interface but produces a non-uniform potential at the NP-surface that may be unrealistic. Unlike many of the simulations discussed in previous sections to isolate polymer dynamics, the NPs in these simulations are free to diffuse and their MSD can be directly measured. The NPs in these simulations tend to aggregate if there are more than one in the simulation and weak NP-polymer interactions, and single NP simulation suffer from poor statistics for NP dynamics, especially at long times. So, to access the diffusive regime, the NPs are typically smaller than the chain size ($R_{NP} < R_g$) or the M_w is small.

6.3. Diffusion in athermal and weakly interacting PNCs

PNCs without NP-polymer enthalpic attractions and with dilute NP concentrations are the simplest PNCs for theoretical predictions [211–213,215,216,218]. At short length scales ($\sim 2R_{NP}$) and fast time scales, scaling descriptions [212] and force-level statistical dynamical theory [213] propose NP caging in the correlation mesh on the order of b or d_{tube} in entangled melts [211,216]. In this regime, relaxations of the surrounding polymer environment lead to random Brownian NP diffusion at longer length-scales ($>2R_{NP}$). This type of motion has been observed in NP-polymer solutions through non-Gaussian dynamics [226] and in the melt through subdiffusion at short length and times scales [227]. Specifically in entangled polymer melts when $R_{NP} \sim d_{tube}$, NPs are predicted to hop between the entanglement network [212,213]. For larger NPs ($R_{NP} \gg R_g$), NPs are unable to escape the entanglement network until it fully relaxes, which decreases the likelihood of this mechanism and leads to slower SE diffusion.

For small NPs ($R_{NP} < R_g$) regardless of the chain length, NP diffusion does not require full chain relaxation, so diffusion is fast relative to $D_{SE}(\eta_0, R_{NP})$. To further understand NP diffusion in entangled polymers, Schweizer and coworkers developed a microscopic, force-level, self-consistent generalized Langevin equation (SCGLE) approach to quantitatively predict the diffusion of repulsive or athermal NPs as a function of NP size and molecular weight

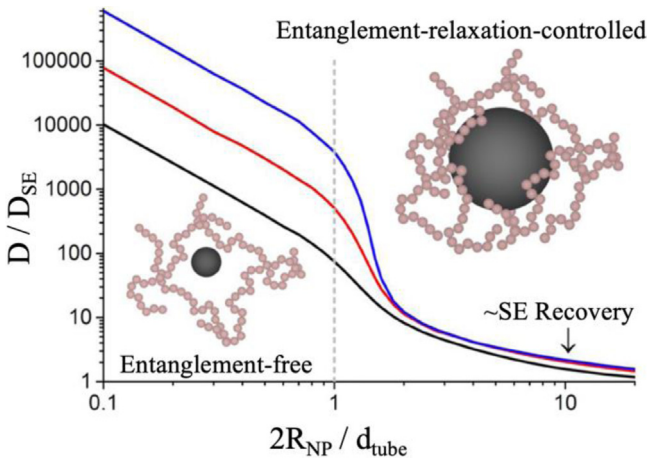

Fig. 14. Self-consistent generalized Langevin equation (SCGLE) predictions for repulsive NP diffusion relative to SE behavior in entangled polymer melts as a function of NP size, R_{NP}, relative to the tube diameter, d_{tube}, for $N/N_e = 4$ (black), 8 (red), and 16 (blue) [216]. Copyright 2015. (For interpretation of the references to color in this figure legend, the reader is referred to the web version of this article.)
Adapted with permission from the American Chemical Society.

[216]. Importantly, this theory does not consider hopping but predicts that particle motion is coupled to the entanglement network dynamics, even if the R_{NP} exceeds the entanglement mesh size. As shown in Fig. 14, for $2R_{NP} \geq \sim 10 d_{tube}$, D_{SE} from Eq. (4) approximately captures the diffusion of repulsive NPs in a polymer melt. For smaller NPs, especially $2R_{NP} < d_{tube}$, NPs diffuse faster than the SE prediction, particularly for smaller NPs in more entangled polymers, because they are influenced by smaller length scale polymer relaxations.

The SCGLE theoretical predictions [216] in Fig. 14 are in reasonable quantitative agreement with coarse-grained MD simulations [228] in unentangled and lightly entangled polymers for $0.1 < 2R_{NP}/d_{tube} < 2$. In this comparison, the authors establish that athermal NP motion is controlled by polymer constraint release wherein NPs are trapped until the polymer environment on the order of $2R_{NP}$ relaxes. Although the hopping mechanism was not observed in these simulations [228], it is expected in highly entangled systems with small NPs ($2R_{NP} \sim d_{tube}$ and $N \gg N_e$). MD simulations have also been used to systematically study repulsive or weakly interacting NP diffusion in the dilute limit as a function of NP size [124,166,195,228–232], polymer M_w [195,228–230,232], NP concentration [124,195,229], surface structure [231], and NP shape [233]. In general, the MD results are consistent with theoretical calculations, in that the diffusion of small NPs or NPs in well-entangled polymers exhibit faster diffusion than the SE prediction. As NP concentration increases, NPs begin to interact and the viscosity of the melt increases, leading to a diffusion coefficient that is reduced relative to the dilute limit [195,229].

Stokes-Einstein enhancements (as predicted in Fig. 14) have been experimentally realized in a variety of weakly interacting PNC systems, especially for small NPs in well-entangled polymers. For example, early XPCS measurements of quantum dots ($2R_{NP}/d_{tube} \sim 0.7$) in PS ($N/N_e \sim 12$) revealed SE enhancements of ~200 with only a subtle dependence on temperature; this is ~100 times slower than predicted in Fig. 14 [234]. In a systematic study of NP size using a modified fluctuation correlation spectroscopy technique, SE enhancements of ~10–2000 were measured for gold NPs with $2R_{NP}/d_{tube} \sim 0.8$–3.3 in well-entangled poly(butyl methacrylate) (PBMA) [221,235]. While these results qualitatively agreed with SCGLE predictions, they did not quantitatively capture the transition around $2R_{NP} \sim d_{tube}$. More recently, using SPT of non-attractive quantum dots in PPG ($2R_{NP}/d_{tube} \sim 2.6$), Gaussian

dynamics were observed at all time-scales studied and SE diffusion was observed ($D \sim D_{SE}$) in unentangled and lightly entangled melts (up to $N/N_e \sim 2.8$) [225]. To date, the theoretical curves in Fig. 14 remain largely unverified experimentally, in part due to the difficulty of dispersing athermal or repulsive NPs in a polymer melts and the challenge of systematically accessing a broad range and relevant values of $2R_{NP}/d_{tube}$ and N/N_e.

One way to improve the dispersion of athermal NPs in a polymer melt is to use grafted NPs, which also alters the NP diffusion coefficient. For example, using athermal grafted NPs with $2R_{NP}<d_{tube}$, the diffusion coefficient measured by RBS was found to be slower than predicted by Eq. (4) and in stark contrast to Fig. 14 [236]. By comparing to field theory calculations, this slowing was attributed to the larger hydrodynamic radius caused by interpenetration of matrix chains and grafted polymer. Interestingly, SE behavior was recovered by using an effective radius, $R_{eff} > R_{NP}$, to account for the presence of grafted chains [236]. This effect was also observed in MD simulations [231].

The dynamics of non-spherical NPs in entangled and unentangled polymer melts has received less attention [203,233,237,238]. The center of mass diffusion coefficient (D_{CM}) of a nanorod with dimensions L and R_{NP} is often described as a combination of diffusion coefficients perpendicular ($D_\perp$) and parallel ($D_\parallel$) to the long axis, both of which follow the form of Eq. (4) [239]:

$$D_{CM} = \frac{D_\parallel}{3} + \frac{2D_\perp}{3} = \left(\frac{kT}{6\pi\eta L}\ln\left[\frac{L}{2R_{NP}}\right]\right) + \left(\frac{kT}{6\pi\eta L}\ln\left[\frac{L}{2R_{NP}}\right]\right)$$
$$= \frac{kT}{3\pi\eta L}\ln\left[\frac{L}{2R_{NP}}\right] \quad (5)$$

This equation is known to describe the diffusion of nanorods in a simple liquid with L and R_{NP} larger than the characteristic length scale of the liquid [240], and much like Eq. (4) for spherical NPs, it is expected to breakdown for small NRs in an entangled polymer melt. Using RBS measurements to study TiO_2 NR diffusion in well-entangled PS ($2R_{NP}<d_{tube}$), the measured NR diffusion coefficient was faster than expected from Eq. (5), reaching enhancements of ~1000 at $M/M_e \sim 100$ [203]. The observed scaling of $D_{CM} \sim M_w^{-1.4}$ implies that NR diffusion is decoupled from the chain-scale viscosity, likely because the NR diameter facilitates NR relaxations within the entanglement network. In MD simulations designed to mimic this experimental system, a hop-like mechanism was identified at long-times when $2R_{NP}<d_{tube}$, although the MD simulations over-predict the NR diffusion coefficient in well-entangled polymer melts [233].

We also note that NP diffusion in dilute and concentrated solutions has also been studied and these three-component systems are analogous to melts, although with additional complex interactions and different confining length scales [211,215,216,219]. NP diffusion has been measured in several polymer solutions with a variety of techniques including XPCS, SPT, and FCS [222,241–245]. The relevant viscosity in NP-polymer solutions depends on the NP and polymer concentrations and the interactions between the NP, solvent, and polymer. Generally, insights regarding NP diffusion from NP-polymer solutions can be used to inform NP diffusion in polymer melts (and visa versa) and may be relevant to understand PNC fabrication from solution.

6.4. Diffusion in attractive PNCs

Although athermal and spherical NPs in a polymer melt can be considered the simplest PNC system, PNC systems with strong NP-polymer attraction have a number of practical advantages so understanding the role of NP-polymer interaction on NP diffusion is critical. Early theories considered the effect of NP-polymer attraction in terms of interfacial polymer packing [215], while more recent descriptions introduce two competing mechanisms: "core-shell" diffusion and "vehicular" diffusion [214]. In core-shell diffusion, which dominates for $R_{NP} > R_g$, adsorbed polymers diffuse along with the NP, thereby increasing the hydrodynamic size ($R_{eff} \approx R_{NP} + R_g$) and slowing diffusion relative to SE behavior [214]. In vehicular diffusion, which dominates for $R_{NP} < R_g$, NPs diffuse with the local polymer environment until successive desorption and readsorption events ("hops") lead to decoupled polymer and NP dynamics, thereby enhancing NP diffusion relative to SE [214].

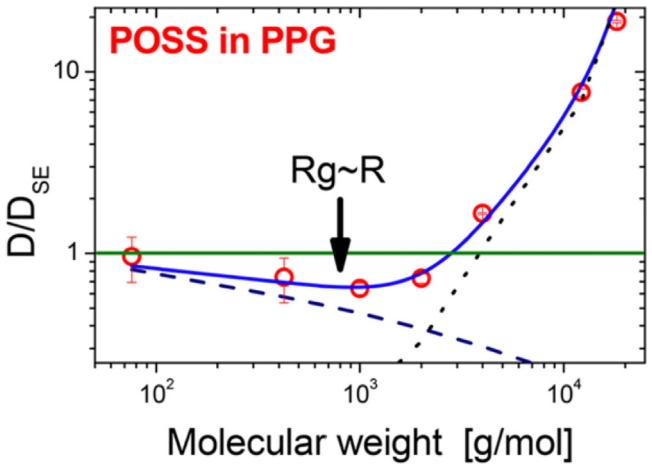

Fig. 15. Crossover from core shell diffusion ($D < D_{SE}$) to vehicle diffusion ($D > D_{SE}$) for OAPS diffusion in PPG as a function of molecular weight [246]. Copyright 2018. Adapted with permission from the American Chemical Society.

The transition between core-shell diffusion and vehicular diffusion has been observed as a function of molecular weight [246] (Fig. 15) and NP size [109,208]. As shown in Fig. 15 for amine-functionalized OAPS diffusion in PPG as measured via DLS, the small NPs ($2R_{NP} \sim 2$ nm) diffuse via core-shell diffusion ($D < D_{SE}$) in short, unentangled melts and via vehicle diffusion ($D > D_{SE}$) in longer, lightly entangled melts [246]. The observed crossover corresponds to where $R_{NP} \sim R_g$, $N \sim N_e$, and when $D_{NP} \sim D_{poly}$. These experimental results are consistent with observations via MD simulations designed to mimic the OAPS/PPG system and the previously described theory [214,246].

Core-shell diffusion [208] and vehicular diffusion [109] have also been observed in well-entangled P2VP melts using RBS and attractive NPs of different size. For 26-nm diameter SiO_2 in P2VP ($2R_{NP} > d_{tube}$), the measured diffusion coefficient was slower than predicted by Eq. (4) and the difference was found to increase with M_w [208]. The difference between D_{NP} and D_{SE} was quantitatively accounted for by an increased hydrodynamic radius that was found to scale with $M_w^{1/2}$ [208], as predicted in core-shell diffusion and also observed in PPG-based attractive PNCs [225,246]. For attractive OAPS in P2VP ($2R_{NP} < d_{tube}$), vehicle diffusion was observed when the timescale and M_w-dependence of NP diffusion was compared to the those of polymer segmental relaxations and chain diffusion [109]. As shown in Fig. 16, OAPS relaxations were found to scale weakly with $M_w^{0.7}$, fall between segmental relaxations and relaxations of entanglement strands, and D/D_{SE} enhancements were found to reach $\sim 10^4$ at $N/N_e \sim 20$ (not shown) [109]. Together, these experimental observations are consistent with vehicle diffusion, where a similar M_w scaling is predicted theoretically and observed in simulations [214].

The diffusion of attractive NPs in a polymer melt has also been probed with atomistic [247–249] and coarse-grained [124,166,192,214,229,250,251] MD simulations. For small fullerenes, NP diffusion in various polymers [247,248] can be observed at microsecond timescales with atomistic detail where

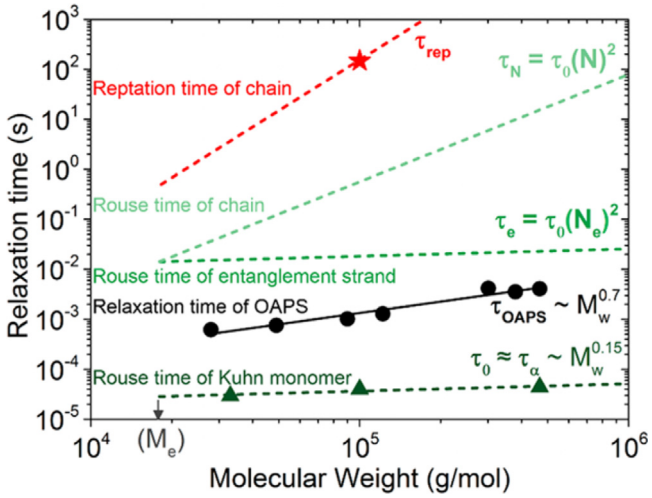

Fig. 16. Comparison of relaxation times for poly(2-vinylpyridine) (P2VP) at various length-scales and attractive OAPS NPs as a function of P2VP molecular weight. The Rouse times of a Kuhn monomer (τ_0, BDS) and P2VP reptation time (τ_{rep}, ERD) were measured on bulk P2VP. OAPS relaxation times (τ_{OAPS}) are calculated directly from RBS measurements. All measurements are made at 140 °C [109]. Copyright 2019. Reproduced with permission from the American Chemical Society.

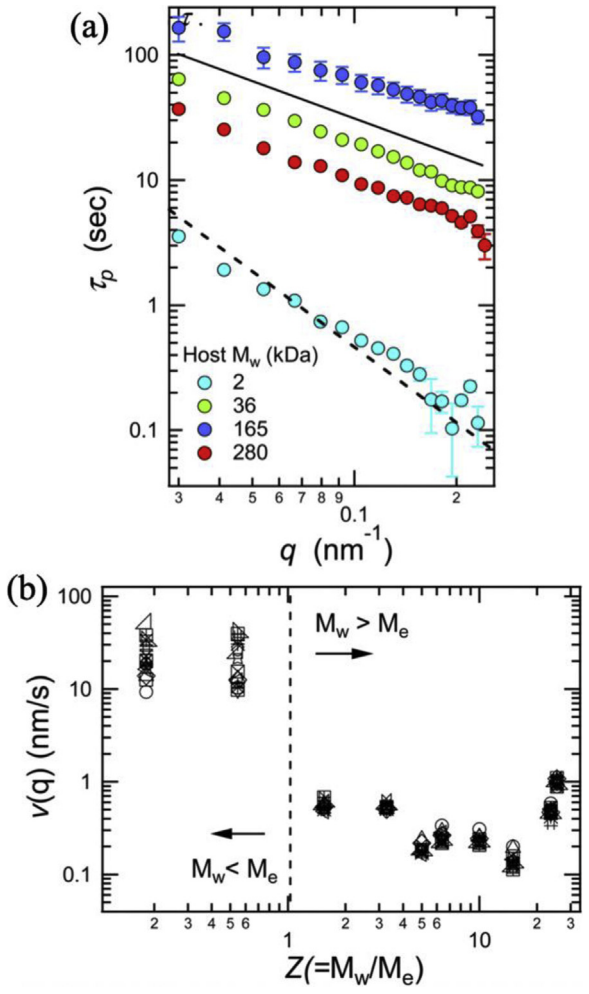

Fig. 17. (a) Nanoparticle relaxation time as a function of q for PEG functionalized SiO_2 in PMMA of varying molecular weight. Solid line denotes superdiffusion (q^{-1}) and dashed line denotes Brownian diffusion (q^{-2}). (b) NP velocity extracted as the slope of (a) as a function of entanglements per chain [159]. Copyright 2016. Adapted with permission from the American Chemical Society.

only one fullerene is included to prevent fullerene aggregation and crystallization. Hopping diffusion was observed in attractive fullerene-polymer melts, such as polyimide [248] or polystyrene (PS) [247], and absent in a non-interacting polypropylene (PP) [247] melt. The comparison of fullerene dynamics in PS and PP shows NP hopping occurs when small NPs adsorb to and desorb from polymer segments, as predicted in vehicle diffusion [247]. Fickian diffusion occurs in both cases at long times, and NP diffusion is slower in more attractive melts [247]. For larger NPs using coarse-grained MD simulations, NP diffusion is observed to be systematically slower for polymer melts with increased NP-polymer interaction, although the degree to which NP diffusion is slowed depends on system-specific parameters such as NP size and interaction strength, among other parameters [124,229,250]. Although most PNC simulations apply NP-polymer interaction through a LJ potential, which can be considered comparable to physical bonding in PNCs, the case of ionic interactions was also studied using MD simulations [251].

6.5. Non-diffusive NP dynamics

Non-diffusive NP dynamics, characterized by MSD $\sim t^{\alpha}$ where $\alpha \neq 1$, is predicted at length- and time-scales before the diffusive regime, such as ballistic motions [38,211–213]. As previously mentioned, subdiffusion ($\alpha < 1$) is predicted for $2R_{NP} > b$ due to the caging of NPs within the correlation network of polymer melts (on the order of b) or the entanglement mesh (on the order of d_{tube}) [212,213]. Experimentally, a crossover from subdiffusion to Fickian diffusion was observed at length scales of $\sim R_{NP}$ using NSE measurements and PEG-functionalized polyhedral oligomeric silsesquioxane dispersed in PEG [227]. This is consistent with the aforementioned theory by Rubinstein and coworkers [211]. In general, this regime is largely unexplored, especially for larger NPs, because observations of motion on the order of or less than R_{NP} in the melt necessitates excellent spatial and temporal resolution and unique length- and time-scales.

Non-diffusive NP dynamics have been widely reported in XPCS in various PNC systems and experimental conditions [131,159,252–265]. Systematic measurements of ~100 nm-diameter PS-grafted SiO_2 NP relaxations (τ_{NP}) in unentangled PS as a function of M_w revealed a temperature dependence to the stretching (or compressing) exponent, γ, on the intermediate scattering function (ISF) and the scaling of n, where $\tau_{NP} \sim q^{-n}$ [259]. For example, sub-diffusion ($n > 2$, $\gamma < 1$) is observed at high temperatures, super-diffusion ($n < 2$, $\gamma > 1$) is observed at lower temperatures, and the crossover is at $1.25T_g$ where Brownian diffusion is observed ($n \sim 2$, $\gamma \sim 1$) [259]. In another XPCS study of attractive 11 nm-diameter PEG-grafted SiO_2 NPs dispersed in PMMA of varying molecular weight, Brownian diffusion is observed in unentangled melts but superdiffusion ($n = 1$, $\tau_{NP} \sim q^{-1}$) is observed above the entanglement molecular weight and the NP velocity is reasonably independent of M_w (Fig. 17) [159]. Observations of nondiffusive NP dynamics have also been reported in PNCs containing dilute [159] and concentrated [262,263] NP volume fractions, grafted [159,259] and bare [261] NPs, athermal [259,260] and attractive [159,260,261] interactions, and under various measurement conditions [252]. Interestingly however, Brownian diffusion has also been observed in XPCS of various PNC systems and conditions [234,266,267].

The origins of anomalous NP dynamics in XPCS remain somewhat unclear. Superdiffusion, akin to a velocity, may occur when a probe experiences kinetic forces without drag forces (ballistic motion) or when a probe interacts with a gradient or field, among other scenarios. Fundamentally, XPCS measures the ensemble-averaged characteristic decorrelation time of the sample electron

density distribution as a function of wave-vector, q [268]. Structural decorrelation on the order of $2\pi/q$ does not require NP diffusion on the order of $2\pi/q$, so the diffusion length can be somewhat unclear in XPCS. However, since XPCS samples length-scales of beyond 100 nm, it is unlikely that the observed super-diffusion rises from probing short-length scale ballistic motions, which are likely «R_{NP}. Some authors surmise that superdiffusive dynamics show the NPs are coupling to internal stress fields, either caused by nonequilibrium and kinetically trapped chain conformations and stress fields in the PNCs or deformation caused by particle motion, both of which can provide elastic energy leading to superdiffusion [159,262,264]. This claim remains debated. Other authors surmise that observed non-diffusive motion results from NP-NP correlations, even in the dilute NP limit when no clear structure factor peak is observed. However, an apparent molecular weight effect in PNCs with similar structure (Fig. 17) and diffusive measurements in lightly aggregated PNCs indicate that NP-NP correlations are not the predominant origin of anomalous dynamics [159,234,261–263]. As a final note, XPCS requires high-brilliance X-ray radiation for prolonged periods of time, and although beamlines monitor sample degradation and try to reduce exposure time and flux, the potential impact of beam damage (albeit largely unknown) has been noted [269–271]. Future studies should aim to further understand the origin of this non-diffusive behavior and develop new and complimentary methods to systematically probe NP motion on similar timescales and compare directly to XPCS.

7. Future outlook

7.1. Role of NP-polymer enthalpic interactions

MD simulations (such as those presented in Fig. 7) have demonstrated that the NP-polymer interaction is a critical parameter that can dictate segmental dynamics from faster than bulk to much slower than bulk. A thorough and detailed experimental realization of this concept and the understanding of other NP and polymer dynamic processes remains to be developed. To isolate the role of NP-polymer interactions, a set of PNCs must be developed to maximize differences in NP-polymer interaction while minimizing differences in other parameters including NP surface chemistry or structure, various polymer properties, and NP dispersion. This experimental goal presents a paradox in that exploring the role of NP-polymer interactions on interfacial behavior necessitates large NP-polymer surface area, while systems devoid of favorable interaction tend to aggregate, even at low φ_{NP}, which decreases the NP-polymer surface area. Although changes in dispersion state may still exist, the NP-polymer interaction can be tuned by NP surface functionalization, matrix chemistry, or brush polymer. Future studies need to deconvolute the effects of NP-polymer interaction, polymer-accessible NP surface area, and other properties in a set of systematic PNCs, so to provide a unified view of polymer dynamics near various NP surfaces. In another potential approach, systematic studies of polymer infiltrated into nanopores with well-defined surface chemistry present a way to study multi-scale dynamics at interfaces with different interactions. This approach may provide valuable insights into PNC dynamics while circumventing concerns with NP dispersion state.

Of particular interest with respect to NP-polymer interaction is the structure and dynamics within the bound polymer layer, as discussed in Section 3.2. For systems with strong NP-polymer interaction, such as P2VP/SiO_2, a bound layer with reduced dynamics at multiple length-scales is well-established [65,208,210,272]. PNCs with repulsive interactions typically exhibit NP aggregation, indicating little adsorbed bound layer experimentally, and according to MD simulations exhibit faster dynamics [119,192]. Demonstrating these faster dynamics remains an experimental challenge and may make new properties and performance attainable. Furthermore, polymer desorption has recently been measured in P2VP/SiO_2 PNCs [206,207] showing polymers remain adsorbed to highly attractive NPs for longer than experimentally accessible time-scales. In systems with modest NP-polymer attraction, it remains unknown whether adsorbed chains remain adsorbed to NPs indefinitely as observed on flat substrates [185,273], or if full desorption and exchange are possible.

Another important aspect of understanding interactions in PNCs involves NPs with grafted polymer chains, which are widely used to improve and control NP dispersion in PNCs [11,12,33]. The use of grafted NPs expands the already expansive parameter space inherent to PNCs. More work is needed to understand the effects of brush conformation on the multiscale dynamics in all-matrix PNCs and traditional PNCs with grafted NPs by systematically studying dynamics as a function of σ_{graft}, grafted M_w, and R_{NP}, as well as the multiple enthalpic interactions (e.g. NP-graft, NP-polymer, and graft-polymer).

7.2. Understanding the hierarchy of dynamics in PNCs

The majority of research papers have focused on a single dynamic process in a specific PNC system. To fully describe the hierarchy of polymer and nanoparticle dynamics, a more encompassing and multi-faceted approach is required, in general. The experimental reports which have studied multiple polymer processes or polymer and nanoparticle dynamics together, have particularly advanced the understanding of coupled dynamics in PNC systems [108,109,139,142,151]. In contrast, measurements of a single dynamic process in a unique PNC system or after unique processing conditions are unable to develop broadly-applicable mechanistic understandings of PNCs.

In many PNC systems, especially those with small NPs and high M_w polymers or strong NP-polymer interactions, NP and polymer dynamics overlap and separating these dynamic processes is often challenging. Recent reports highlight the unique dynamic behaviors when NPs are highly mobile relative to the polymer: drastic changes to the glass transition temperature, homogeneously slow segmental dynamics in the melt state, and a commensurate slowing of chain dynamics [108,109]. It remains an open question if these effects are simply a result of large polymer-NP interface resulting from small NPs [99] or if the vehiclar mechanism of NP diffusion fundamentally and uniquely alters other dynamic processes [214]. In general, our understanding of NP motion and how NPs affect polymer dynamics at various length-scales is critical to design PNC materials and anticipate their performance in various properties. Furthermore, it is critical to consider each dynamic process in PNCs synergistically and to consider how one may influence another.

7.3. Role of processing parameters for kinetically trapping PNCs

Despite the decades of research, it remains unclear if PNCs in general reach their equilibrium morphology or if they are often in a kinetically trapped state. This delineation is of critical importance. First, if PNCs cannot access their equilibrium state, comparison with current equilibrium-based theory and simulation require caution and new theory and simulation efforts are needed to incorporate nonequilibrium effects. Second, if PNCs are in kinetically trapped states, engineers should be able to use processing methods and parameters to further tune and control PNC macroscopic properties. Third, because the diversity of processing conditions reported in literature, such as solvent quality, species concentrations during preparation, and annealing protocols, is extensive, comparisons between different experiments is suspect when the PNC morphology, structure, or polymer conformations are likely different.

In fact, there is evidence of nonequilibrium effects in common PNC research. For example, theoretically predicted and simulated phase diagrams for PNCs differ from those experimentally observed [97,98]. Even more, it has been shown that the final NP dispersion states [274,275] depend on the solvent quality used during fabrication. Even more recently, the bound layer structure and properties were analyzed in PNCs made from good and poor solvent [70]. In these PEO/SiO_2 PNCs, a thicker bound layer and more perturbed dynamics were observed in PNCs fabricated from poor solvent (ethanol) relative to a good solvent (water) [70]. These results highlight that these complex materials often fail to sample their equilibrium morphologies or access the global minimum on their energetic landscape. Instead, the dynamics and properties depend on the way the samples are fabricated. This gives researchers an opportunity to control properties and study PNCs with new microscopic structure, while fundamental and systematic studies are also required to understand the effective potential landscape and states accessed. The significant role of PNC processing also hinders the use of machine learning to extract insights by combining datasets without complete processing methods. For this new approach to be impactful, more fundamental work is required to fully understand the potential landscape, influence of processing, and role of various parameters on polymer dynamics.

7.4. Approach to PNC research

The broad parameter space presented by PNCs is among the reasons fundamental nanocomposites research is important and their applications are plentiful. This broad parameter space is also responsible for one of the main challenges to the field. It is sometimes inappropriate to compare experimental observations or measurements from either different PNC systems or different techniques because there are often confounding variables that complicate the comparison. For example, as discussed in Section 7.3, the same PNC systems can exhibit different NP morphologies, and therefore microscopic dynamics and macroscopic properties, as a result of the processing parameters [274,275]. In addition, as others have discussed [29,36,54,55,76,77], different measurements probe or sample properties differently, and consideration of this fact is necessary to develop accurate descriptions of physical phenomena. Thus, it is important to note that not every observation is ubiquitous in the PNC community and caution should be used when comparing across different PNC systems and experiments. However, comparisons are essential to develop and validate theories and mechanistic descriptions, so, it is important for future reports to facilitate such comparisons. First and foremost, authors must include specific details regarding preparation and measurements in future publications and report raw data when relevant. Second, the robustness of conclusions and effects can be improved by reporting the observation across different PNC materials systems, measurement techniques, or experimental conditions. These complimentary measurements, while potentially difficult experimentally, will help identify confounding variables and facilitate a broader appreciation in the PNC community.

Another important aspect of PNC research that remains a challenge is narrowing the gap between simulations and experiments, especially coarse-grained molecular dynamics simulations. MD simulations present the unique opportunity to mechanistically and quantitatively understand PNC dynamic processes, rapidly explore the dense parameter space, and isolate, control, and measure individual variables and properties. For maximum impact, the goal should be to directly verify simulations with experiments which will help make simulations more predictive and their results attainable experimentally. Although the relation of Kremer-Grest parameters to experimental parameters in polymer melts has been reported [63], several PNC parameters remain unclear. For example, the NP-polymer interaction is often modelled by a LJ potential, but it remains unclear the range of interaction strengths (ε) that match experimental systems. Furthermore, the appropriate structure of the NP that eliminates artificial packing and enhanced density at the interface and properly simulates the energetic landscape at the NP-polymer interface remains unclear, partly due to a limited understanding of NP interfaces experimentally. In the future, specific parameters and measurements need to be investigated and developed to verify and directly compare experimental measurements with simulated PNC systems, including the role of processing.

Much of the work discussed in this review is fundamental in nature, which is important to inform the design, development, and fabrication of new PNC materials. Now, more effort needs to be dedicated to developing predictive models and proxies for real property measurements. It is important to understand to what effect the dynamic changes measured in PNCs affect macroscopic properties, as discussed in Section 2.2. For example, if the addition of NPs slows the segmental relaxation rate near the NPs by 50%, to what extent are the permeabilities of small molecules reduced for membrane applications? While this is a difficult challenge, the impact of such efforts cannot be overstated. Even though most properties are not directly and solely related to dynamic processes, relating the dynamic properties discussed in this review to tangible properties will advance PNCs in various applications.

Declaration of Competing Interest

The authors declare that they have no known competing financial interests or personal relationships that could have appeared to influence the work reported in this paper.

Acknowledgements

The authors acknowledge financial support from ACS Petroleum Research Fund57405-ND7, NSF-CBET #1706014, and DOE-BES-DE-SC0016421.

References

[1] Balazs AC, Emrick T, Russell TP. Nanoparticle polymer composites: where two small worlds meet. Science 2006;314:1107–10.
[2] Winey KI, Vaia RA. Polymer nanocomposites. MRS Bull 2007;32:314–22.
[3] Arepalli S, Moloney P. Engineered nanomaterials in aerospace. MRS Bull 2015;40:804–11.
[4] Kumar SK, Benicewicz BC, Vaia RA, Winey KI. 50th anniversary perspective: are polymer nanocomposites practical for applications? Macromolecules 2017;50:714–31.
[5] Fernandes NJ, Koerner H, Giannelis EP, Vaia RA. Hairy nanoparticle assemblies as one- component functional polymer nanocomposites: opportunities and challenges. MRS Commun 2013;3:13–29.
[6] Paul DR, Robeson LM. Polymer nanotechnology: nanocomposites. Polymer 2008;49:3187–204.
[7] Pandey N, Shukla SK, Singh NB. Water purification by polymer nanocomposites: an overview. Nanocomposites 2017;3:47–66.
[8] Kumar SK, Krishnamoorti R. Nanocomposites: structure, phase behavior, and properties. Annu Rev Chem Biomol Eng 2010;1:37–58.
[9] Krishnamoorti R. Strategies for dispersing nanopar ticles in polymers. MRS Bull 2007;32:341–7.
[10] Hore MJA, Composto RJ. Functional polymer nanocomposites enhanced by nanorods. Macromolecules 2014;47:875–87.
[11] Green PF. The structure of chain end-grafted nanoparticle/homopolymer nanocomposites. Soft Matter 2011;7:7914–26.
[12] Kumar SK, Jouault N, Benicewicz B, Neely T. Nanocomposites with polymer grafted nanoparticles. Macromolecules 2013;46:3199–214.
[13] de Azeredo HMC. Nanocomposites for food packaging applications. Food Res Int 2009;42:1240–53.
[14] Merkel TC, Freeman BD, Spontak RJ, He Z, Pinnau I, Meakin P, et al. Ultrapermeable, reverse-selective nanocomposite membranes. Science 2002;296:519–23.
[15] Mutiso RM, Winey KI. Electrical properties of polymer nanocomposites containing rod-like nanofillers. Prog Polym Sci 2015;40:63–84.

[16] Byrne MT, Guin'Ko YK. Recent advances in research on carbon nanotube - polymer composites. Adv Mater 2010;22:1672–88.
[17] Croce F, Appetecchi GB, Persi L, Scrosati B. Nanocomposite polymer electrolytes for lithiumbatteries. Nature 1998;394:456–8.
[18] Kulkarni DD, Choi I, Singamaneni SS, Tsukruk VV. Graphene oxide-polyelectrolyte nanomembranes. ACS Nano 2010;4:4667–76.
[19] Hore MJA, Composto RJ. Nanorod self-assembly for tuning optical absorption. ACS Nano 2010;4:6941–9.
[20] Raftopoulos KN, Pielichowski K. Segmental dynamics in hybrid polymer/POSS nanomaterials. Prog Polym Sci 2016;52:136–87.
[21] Kim H, Abdala AA, MacOsko CW. Graphene/polymer nanocomposites. Macromolecules 2010;43:6515–30.
[22] Hu X, Zhang W, Si M, Gelfer M, Hsiao B, Rafailovich M, et al. Dynamics of polymers in organosilicate nanocomposites. Macromolecules 2003;36:823–9.
[23] Chrissopoulou K, Anastasiadis SH. Effects of nanoscopic-confinement on polymer dynamics. Soft Matter 2015;11:3746–66.
[24] Anastasiadis SH, Chrissopoulou K, Frick B. Structure and dynamics in polymer/layered silicate nanocomposites. Mater Sci Eng B 2008;152:33–9.
[25] Kumar SK, Ganesan V, Riggleman RA. Perspective: outstanding theoretical questions in polymer-nanoparticle hybrids. J Chem Phys 2017;147, 020901/1-19.
[26] Lin CC, Parrish E, Composto RJ. Macromolecule and particle dynamics in confined media. Macromolecules 2016;49:5755–72.
[27] Richter D, Kruteva M. Polymer dynamics under confinement. Soft Matter 2019;15:7316–49.
[28] Simmons DS. An emerging unified view of dynamic interphases in polymers. Macromol Chem Phys 2016;217:137–48.
[29] Cheng S, Carroll B, Bocharova V, Carrillo JM, Sumpter BG, Sokolov AP. Focus: structure and dynamics of the interfacial layer in polymer nanocomposites with attractive interactions. J Chem Phys 2017;146, 203201/1-14.
[30] Volgin IV, Larin SV, Lyulin SV. Diffusion of nanoparticles in polymer systems. Polym Sci Ser A Chem Phys 2018;60:122–34.
[31] Peng H, Nieuwendaal R, Soles CL. Polymer dynamics in constrained geometries. In: Matyjaszewski K, Möller M, editors. Polymer science: a comprehensive reference, vol. 7. Amsterdam: Elsevier BV; 2012. p. 345–76.
[32] Karatrantos A, Composto RJ, Winey KI, Kröger M, Clarke N. Modeling of entangled polymer diffusion in melts and nanocomposites: a review. Polymers 2019;11, 876/1-29.
[33] Hore MJA. Polymers on nanoparticles: structure & dynamics. Soft Matter 2019;15:1120–34.
[34] Tjong SC. Structural and mechanical properties of polymer nanocomposites. Mater Sci Eng R Rep 2006;53:73–197.
[35] Rubinstein M, Colby RH. Polymer physics. New York: Oxford University Press; 2003, 454 pp.
[36] Priestley RD, Cangialosi D, Napolitano S. On the equivalence between the thermodynamic and dynamic measurements of the glass transition in confined polymers. J Non Cryst Solids 2015;407:288–95.
[37] Arrese-Igor S, Arbe A, Frick B, Colmenero J. Glassy dynamics of polystyrene by quasielastic neutron scattering. Macromolecules 2011;44:3161–8.
[38] Wyart FB, De Gennes PG. Viscosity at small scales in polymer melts. Eur Phys J E 2000;1:93–7.
[39] Genix AC, Bocharova V, Kisliuk A, Carroll B, Zhao S, Oberdisse J, et al. Enhancing the mechanical properties of glassy nanocomposites by tuning polymer molecular weight. ACS Appl Mater Interfaces 2018;10: 33601–10.
[40] Chen Q, Gong S, Moll J, Zhao D, Kumar SK, Colby RH. Mechanical reinforcement of polymer nanocomposites from percolation of a nanoparticle network. ACS Macro Lett 2015;4:398–402.
[41] Yang S, Akcora P. Deformation of chemically heterogeneous interfacial layers of polymer nanocomposites. ACS Macro Lett 2019;8:1635–41.
[42] Mogurampelly S, Ganesan V. Influence of nanoparticle surface chemistry on ion transport in polymer nanocomposite electrolytes. Solid State Ion 2016;286:57–65.
[43] Bilchak CR, Buenning E, Asai M, Zhang K, Durning CJ, Kumar SK, et al. Polymer-grafted nanoparticle membranes with controllable free volume. Macromolecules 2017;50:7111–20.
[44] Takahashi S, Paul DR. Gas permeation in poly(ether imide) nanocomposite membranes based on surface-treated silica. Part 1: without chemical coupling to matrix. Polymer 2006;47:7519–34.
[45] Merkel TC, Freeman BD, Spontak RJ, He Z, Pinnau I, Meakin P, et al. Sorption, transport, and structural evidence for enhanced free volume in poly(4-methyl-2-pentyne)/fumed silica nanocomposite membranes. Chem Mater 2003;15:109–23.
[46] Jhalaria M, Buenning E, Huang Y, Tyagi M, Zorn R, Zamponi M, et al. Accelerated local dynamics in matrix-free polymer grafted nanoparticles. Phys Rev Lett 2019;123, 158003/1-6.
[47] Capadona JR, Shanmuganathan K, Tyler DJ, Rowan SJ, Weder C. Stimuli-responsive polymer nanocomposites inspired by the sea cucumber dermis. Science 2008;319:1370–5.
[48] Gupta S, Zhang Q, Emrick T, Balazs AC, Russell TP. Entropy-driven segregation of nanoparticles to cracks in multilayered composite polymer structures. Nat Mater 2006;5:229–33.
[49] Böker A, He J, Emrick T, Russell TP. Self-assembly of nanoparticles at interfaces. Soft Matter 2007;3:1231–48.
[50] Rittigstein P, Priestley RD, Broadbelt LJ, Torkelson JM. Model polymer nanocomposites provide an understanding of confinement effects in real nanocomposites. Nat Mater 2007;6:278–82.
[51] Liu R, Guo Y, Odusote G, Qu F, Priestley RD. Core-shell Fe3O4 polydopamine nanoparticles serve multipurpose as drug carrier, catalyst support and carbon adsorbent. ACS Appl Mater Interfaces 2013;5:9167–71.
[52] Mora-Huertas CE, Fessi H, Elaissari A. Polymer-based nanocapsules for drug delivery. Int J Pharm 2010;385:113–42.
[53] Kalwarczyk T, Tabaka M, Holyst R. Biologistics-diffusion coefficients for complete proteome of Escherichia coli. Bioinformatics 2012;28:2971–8.
[54] Robertson CG, Roland CM. Glass transition and interfacial segmental dynamics in polymer-particle composites. Rubber Chem Technol 2011;81:506–22.
[55] Bailey EJ, Griffin PJ, Tyagi M, Winey KI. Segmental diffusion in attractive polymer nanocomposites: a quasi-elastic neutron scattering study. Macromolecules 2019;52:669–78.
[56] Schawe JEK. A comparison of different evaluation methods in modulated temperature DSC. Thermochim Acta 1995;260:1–16.
[57] Kremer F, Schönhals A, editors. Broadband dielectric spectroscopy. Berlin: Springer-Verlag; 2002, 702 pp.
[58] Carroll B, Cheng S, Sokolov AP. Analyzing the interfacial layer properties in polymer nanocomposites by broadband dielectric spectroscopy. Macromolecules 2017;50:6149–63.
[59] Springer T. Quasielastic neutron scattering for the investigation of diffusive motions in solids and liquids. Berlin: Springer-Verlag; 1972, 102 pp.
[60] Richter D, Monkenbusch, Schwahn D. Neutron scattering. In: Matyjaszewski K, Möller M, editors. Polymer science: a comprehensive reference, vol. 7. Amsterdam: Elsevier BV; 2012. p. 331–60.
[61] Saalwächter K, Spiess H. Solid-state NMR of polymers. In: Matyjaszewski K, Möller M, editors. Polymer science: a comprehensive reference, vol. 7. Amsterdam: Elsevier BV; 2012. p. 185–218.
[62] Papon A, Saalwächter K, Schäler K, Guy L, Lequeux F, Montes H. Low-field NMR investigations of nanocomposites: polymer dynamics and network effects. Macromolecules 2011;44:913–22.
[63] Kremer K, Grest GS. Dynamics of entangled linear polymer melts: a molecular-dynamics simulation. J Chem Phys 1990;92:5057–86.
[64] Moll J, Kumar SK. Glass transitions in highly attractive highly filled polymer nanocomposites. Macromolecules 2012;45:1131–5.
[65] Holt AP, Griffin PJ, Bocharova V, Agapov AL, Imel AE, Dadmun MD, et al. Dynamics at the polymer/nanoparticle interface in poly(2-vinylpyridine)/silica nanocomposites. Macromolecules 2014;47:1837–43.
[66] Gong S, Chen Q, Moll JF, Kumar SK, Colby RH. Segmental dynamics of polymer melts with spherical nanoparticles. ACS Macro Lett 2014;3:773–7.
[67] Baeza GP, Dessi C, Costanzo S, Zhao D, Gong S, Alegria A, et al. Network dynamics in nanofilled polymers. Nat Commun 2016;7:1–6.
[68] Harton SE, Kumar SK, Yang H, Koga T, Hicks K, Lee H, et al. Immobilized polymer layers on spherical nanoparticles. Macromolecules 2010;43:3415–21.
[69] Voylov DN, Holt AP, Doughty B, Bocharova V, Meyer HM, Cheng S, et al. Unraveling the molecular weight dependence of interfacial interactions in poly(2-vinylpyridine)/Silica nanocomposites. ACS Macro Lett 2017;6: 68–72.
[70] Oh SM, Abbasi M, Shin TJ, Saalwächter K, Kim SY. Initial solvent-driven nonequilibrium effect on structure, properties, and dynamics of polymer nanocomposites. Phys Rev Lett 2019;123, 167801/1-6.
[71] Papon A, Montes H, Lequeux F, Oberdisse J, Saalwächter K, Guy L. Solid particles in an elastomer matrix: impact of colloid dispersion and polymer mobility modification on the mechanical properties. Soft Matter 2012;8:4090–6.
[72] Füllbrandt M, Purohit PJ, Schönhals A. Combined FTIR and dielectric investigation of poly(vinyl acetate) adsorbed on silica particles. Macromolecules 2013;46:4626–32.
[73] Cheng S, Holt AP, Wang H, Fan F, Bocharova V, Martin H, et al. Unexpected molecular weight effect in polymer nanocomposites. Phys Rev Lett 2016;116, 038302/1-5.
[74] Cheng S, Carroll B, Lu W, Fan F, Carrillo JMY, Martin H, et al. Interfacial properties of polymer nanocomposites: role of chain rigidity and dynamic heterogeneity length scale. Macromolecules 2017;50:2397–406.
[75] Coleman NJ, Craig DQM. Modulated temperature differential scanning calorimetry: a novel approach to pharmaceutical thermal analysis. Int J Pharm 1996;135:13–29.
[76] Ye C, Wiener CG, Tyagi M, Uhrig D, Orski SV, Soles CL, et al. Understanding the decreased segmental dynamics of supported thin polymer films reported by incoherent neutron scattering. Macromolecules 2015;48:801–8.
[77] Glomann T, Schneider GJ, Allgaier J, Radulescu A, Lohstroh W, Farago B, et al. Microscopic dynamics of polyethylene glycol chains interacting with silica nanoparticles. Phys Rev Lett 2013;110, 178001/1-5.
[78] Bansal A, Yang H, Li C, Cho K, Benicewicz BC, Kumar SK, et al. Quantitative equivalence between polymer nanocomposites and thin polymer films. Nat Mater 2005;4:693–8.
[79] Starr FW, Schrøder TB, Glotzer SC. Molecular dynamics simulation of a polymer melt with a nanoscopic particle. Macromolecules 2002;35:4481–92.
[80] Zhang W, Emamy H, Pazmiño Betancourt BA, Vargas-Lara F, Starr FW, Douglas JF. The interfacial zone in thin polymer films and around

nanoparticles in polymer nanocomposites. J Chem Phys 2019;151, 124705/1-9.
[81] Franz C, Lange F, Golitsyn Y, Hartmann-Azanza B, Steinhart M, Krutyeva M, et al. Chain dynamics and segmental orientation in polymer melts confined to nanochannels. Macromolecules 2016;49:244–56.
[82] Krutyeva M, Wischnewski A, Monkenbusch M, Willner L, Maiz J, Mijangos C, et al. Effect of nanoconfinement on polymer dynamics: surface layers and interphases. Phys Rev Lett 2013;110, 108303/1-5.
[83] Krutyeva M, Pasini S, Monkenbusch M, Allgaier J, Maiz J, Mijangos C, et al. Polymer dynamics under cylindrical confinement featuring a locally repulsive surface: a quasielastic neutron scattering study. J Chem Phys 2017;146, 203306/1-11.
[84] Vo LT, Anastasiadis SH, Giannelis EP. Dielectric study of poly(styrene-co-butadiene) composites with carbon black, silica, and nanoclay. Macromolecules 2011;44:6162–71.
[85] Hanakata PZ, Douglas JF, Starr FW. Interfacial mobility scale determines the scale of collective motion and relaxation rate in polymer films. Nat Commun 2014;5:1–8.
[86] Roth CB, Dutcher JR. Glass transition and chain mobility in thin polymer films. J Electroanal Chem 2005;584:13–22.
[87] Priestley RD, Ellison CJ, Broadbelt LJ. Structural relaxation of polymer glasses at surfaces, interfaces, and in between. Science 2005;309:456–60.
[88] Holt AP, Bocharova V, Cheng S, Kisliuk AM, White BT, Saito T, et al. Controlling interfacial dynamics: covalent bonding versus physical adsorption in polymer nanocomposites. ACS Nano 2016;10:6843–52.
[89] Kim SY, Meyer HW, Saalwächter K, Zukoski CF. Polymer dynamics in PEG-silica nanocomposites: effects of polymer molecular weight, temperature and solvent dilution. Macromolecules 2012;45:4225–37.
[90] Askar S, Li L, Torkelson JM. Polystyrene-grafted silica nanoparticles: investigating the molecular weight dependence of glass transition and fragility behavior. Macromolecules 2017;50:1589–98.
[91] Klonos PA, Goncharuk OV, Pakhlov EM, Sternik D, Derylo-Marczewska A, Kyritsis A, et al. Morphology, molecular dynamics, and interfacial phenomena in systems based on silica modified by grafting polydimethylsiloxane chains and physically adsorbed polydimethylsiloxane. Macromolecules 2019;52:2863–77.
[92] Mark C, Holderer O, Allgaier J, Hübner E, Pyckhout-Hintzen W, Zamponi M, et al. Polymer chain conformation and dynamical confinement in a model one-component nanocomposite. Phys Rev Lett 2017;119, 047801/1-5.
[93] Carrillo JMY, Cheng S, Kumar R, Goswami M, Sokolov AP, Sumpter BG. Untangling the effects of chain rigidity on the structure and dynamics of strongly adsorbed polymer melts. Macromolecules 2015;48 :4207–19.
[94] Klonos P, Kyritsis A, Bokobza L, Gun'ko VM, Pissis P. Interfacial effects in PDMS/titania nanocomposites studied by thermal and dielectric techniques. Colloids Surf A 2017;519:212–22.
[95] Akcora P, Kumar SK, García Sakai V, Li Y, Benicewicz BC, Schadler LS. Segmental dynamics in PMMA-grafted nanoparticle composites. Macromolecules 2010;43:8275–81.
[96] Wu S. Phase structure and adhesion in polymer blends: a criterion for rubber toughening. Polymer 1985;26:1855–63.
[97] Hall LM, Jayaraman A, Schweizer KS. Molecular theories of polymer nanocomposites. Curr Opin Solid State Mater Sci 2010;14:38–48.
[98] Hall LM, Anderson BJ, Zukoski CF, Schweizer KS. Concentration fluctuations, local order, and the collective structure of polymer nanocomposites. Macromolecules 2009;42:8435–42.
[99] Emamy H, Kumar SK, Starr FW. Diminishing interfacial effects with decreasing nanoparticle size in polymer-nanoparticle composites. Phys Rev Lett 2018;121, 207801/1-5.
[100] Swenson J, Smalley MV, Hatharasinghe HLM. Mechanism and strength of polymer bridging flocculation. Phys Rev Lett 1998;81:5840–3.
[101] Allegra G, Raos G, Vacatello M. Theories and simulations of polymer-based nanocomposites: from chain statistics to reinforcement. Prog Polym Sci 2008;33:683–731.
[102] Srivastava S, Kotov NA. Composite layer-by-layer (LBL) assembly with inorganic nanoparticles and nanowires. Acc Chem Res 2008;41:1831–41.
[103] Huang YR, Jiang Y, Hor JL, Gupta R, Zhang L, Stebe KJ, et al. Polymer nanocomposite films with extremely high nanoparticle loadings via capillary rise infiltration (CaRI). Nanoscale 2015;7:798–805.
[104] Hor JL, Wang H, Fakhraai Z, Lee D. Effect of physical nanoconfinement on the viscosity of unentangled polymers during capillary rise infiltration. Macromolecules 2018;51:5069–78.
[105] Wang H, Hor JL, Zhang Y, Liu T, Lee D, Fakhraai Z. Dramatic increase in polymer glass transition temperature under extreme nanoconfinement in weakly interacting nanoparticle films. ACS Nano 2018;12:5580–7.
[106] Holt AP, Roland CM. Segmental and secondary dynamics of nanoparticle-grafted oligomers. Soft Matter 2018;14:8604–11.
[107] Roh JH, Tyagi M, Hogan TE, Roland CM. Space-dependent dynamics in 1,4-polybutadiene nanocomposite. Macromolecules 2013;46: 6667–9.
[108] Cheng S, Xie SJ, Carrillo JMY, Carroll B, Martin H, Cao PF, et al. Big effect of small nanoparticles: a shift in paradigm for polymer nanocomposites. ACS Nano 2017;11:752–9.
[109] Bailey EJ, Griffin PJ, Composto RJ, Winey KI. Multiscale dynamics of small, attractive nanoparticles and entangled polymers in polymer nanocomposites. Macromolecules 2019;52:2181–8.
[110] Karatrantos A, Clarke N, Kröger M. Modeling of polymer structure and conformations in polymer nanocomposites from atomistic to mesoscale: a review. Polym Rev 2016;56:385–428.
[111] Lin Y, Liu L, Xu G, Zhang D, Guan A, Wu G. Interfacial interactions and segmental dynamics of poly(vinyl acetate)/silica nanocomposites. J Phys Chem C 2015;119:12956–66.
[112] Klonos P, Bolbukh Y, Koutsiara CS, Zafeiris K, Kalogeri OD, Sternik D, et al. Morphology and molecular dynamics investigation of low molecular weight PDMS adsorbed onto Stöber, fumed, and sol-gel silica nanoparticles. Polymer 2018;148:1–13.
[113] Kirst KU, Kremer F, Litvinov VM. Broad-band dielectric spectroscopy on the molecular dynamics of bulk and adsorbed poly(dimethylsiloxane). Macromolecules 1993;26:975–80.
[114] Klonos P, Kyritsis A, Pissis P. Effects of surface modification and thermal annealing on the interfacial dynamics in core-shell nanocomposites based on silica and adsorbed PDMS. Eur Polym J 2015;70:342–59.
[115] Litvinov VM, Spies HW. 2H NMR Study of molecular motions in polydimethylsiloxane and its mixtures with aerosils. Die Makromol Chem 1991;192:3005–19.
[116] Holt AP, Sangoro JR, Wang Y, Agapov AL, Sokolov AP. Chain and segmental dynamics of poly(2-vinylpyridine) nanocomposites. Macromolecules 2013;46:4168–73.
[117] Tsagaropoulos G, Eisenberg A. Dynamic mechanical study of the factors affecting the two glass transition behavior of filled polymers. Similarities and differences with random ionomers. Macromolecules 1995;28:6067–77.
[118] Natarajan B, Li Y, Deng H, Brinson LC, Schadler LS. Effect of interfacial energetics on dispersion and glass transition temperature in polymer nanocomposites. Macromolecules 2013;46:2833–41.
[119] Starr FW, Douglas JF, Meng D, Kumar SK. Bound layers "Cloak" nanoparticles in strongly interacting polymer nanocomposites. ACS Nano 2016;10:10960–5.
[120] Starr FW, Schrøder TB, Glotzer SC. Effects of a nanoscopic filler on the structure and dynamics of a simulated polymer melt and the relationship to ultrathin films. Phys Rev E 2001;64, 021802/1-6.
[121] Starr FW, Douglas JF. Modifying fragility and collective motion in polymer melts with nanoparticles. Phys Rev Lett 2011;106, 115702/1-4.
[122] Pazmiño Betancourt BA, Douglas JF, Starr FW. Fragility and cooperative motion in a glass- forming polymer-nanoparticle composite. Soft Matter 2013;9:241–54.
[123] Cheng S, Mirigian S, Carrillo JMY, Bocharova V, Sumpter BG, Schweizer KS, et al. Revealing spatially heterogeneous relaxation in a model nanocomposite. J Chem Phys 2015;143, 194704/1-16.
[124] Patti A. Molecular dynamics of spherical nanoparticles in dense polymer melts. J Phys Chem B 2014;118:3731–42.
[125] Berriot J, Lequeux F, Monnerie L, Montes H, Long D, Sotta P. Filler–elastomer interaction in model filled rubbers, a 1H NMR study. J Non Cryst Solids 2002;307–310:719–24.
[126] Golitsyn Y, Schneider GJ, Saalwächter K. Reduced-mobility layers with high internal mobility in poly(ethylene oxide)-silica nanocomposites. J Chem Phys 2017;146, 203303/1-8.
[127] Holt AP, Bocharova V, Cheng S, Kisliuk AM, Ehlers G, Mamontov E, et al. Interplay between local dynamics and mechanical reinforcement in glassy polymer nanocomposites. Phys Rev Mater 2017;1, 062601/1-6.
[128] Kim SA, Mangal R, Archer LA. Relaxation dynamics of nanoparticle-tethered polymer chains. Macromolecules 2015;48:6280–93.
[129] Rishi K, Beaucage G, Kuppa V, Mulderig A, Narayanan V, McGlasson A, et al. Impact of an emergent hierarchical filler network on nanocomposite dynamics. Macromolecules 2018;51:7893–904.
[130] Yang J, Melton M, Sun R, Yang W, Cheng S. Decoupling the polymer dynamics and the nanoparticle network dynamics of polymer nanocomposites through dielectric spectroscopy and rheology. Macromolecules 2020;53:302–11.
[131] Senses E, Ansar SM, Kitchens CL, Mao Y, Narayanan S, Natarajan B, et al. Small particle driven chain disentanglements in polymer nanocomposites. Phys Rev Lett 2017;118, 147801/1-5.
[132] Kröger M. Shortest multiple disconnected path for the analysis of entanglements in two- and three- dimensional polymeric systems. Comput Phys Commun 2005;168:209–32.
[133] Shanbhag S, Kröger M. Primitive path networks generated by annealing and geometrical methods: insights into differences. Macromolecules 2007;40:2897–903.
[134] Karayiannis NC, Kröger M. Combined molecular algorithms for the generation, equilibration and topological analysis of entangled polymers: methodology and performance. Int J Mol Sci 2009;10:5054–89.
[135] Fragiadakis D, Pissis P. Glass transition and segmental dynamics in poly(dimethylsiloxane)/silica nanocomposites studied by various techniques. J Non Cryst Solids 2007;353:4344–52.
[136] Termonia Y. Chain confinement in polymer nanocomposites and its effect on polymer bulk properties. J Polym Sci Part B: Polym Phys 2010;48:687–92.
[137] Zhang Q, Archer LA. Poly(ethylene oxide)/silica nanocomposites: structure and rheology. Langmuir 2002;18:10435–42.
[138] Nusser K, Schneider GJ, Richter D. Microscopic origin of the terminal relaxation time in polymer nanocomposites: an experimental precedent. Soft Matter 2011;7:7988–91.
[139] Mangal R, Srivastava S, Archer LA. Phase stability and dynamics of entangled polymer- nanoparticle composites. Nat Commun 2015;6:1–9.

[140] Tuteja A, Mackay ME, Hawker CJ, Van Horn B. Effect of ideal, organic nanoparticles on the flow properties of linear polymers: non-Einstein-like behavior. Macromolecules 2005;38:8000–11.
[141] Senses E, Faraone A, Akcora P. Microscopic chain motion in polymer nanocomposites with dynamically asymmetric interphases. Sci Rep 2016;6, 29326/1-11.
[142] Bogoslovov RB, Roland CM, Ellis AR, Randall AM, Robertson CG. Effect of silica nanoparticles on the local segmental dynamics in polyvinylacetate. Macromolecules 2008;41:1289–96.
[143] Song Y, Zheng Q. Size-dependent linear rheology of silica filled poly(2-vinylpyridine). Polymer 2017;130:74–8.
[144] Casalini R, Roland CM. Local and global dynamics in polypropylene glycol/silica composites. Macromolecules 2016;49:3919–24.
[145] Mackay ME, Dao TT, Tuteja A, Ho DL, Van Horn B, Kim HC, et al. Nanoscale effects leading to non-Einstein-like decrease in viscosity. Nat Mater 2003;2:762–6.
[146] Batchelor GK. The effect of Brownian motion on the bulk stress in a suspension of spherical particles. J Fluid Mech 1977;83:97–117.
[147] Kalathi JT, Grest GS, Kumar SK. Universal viscosity behavior of polymer nanocomposites. Phys Rev Lett 2012;109, 198301/1-5.
[148] Schneider GJ, Nusser K, Neueder S, Brodeck M, Willner L, Farago B, et al. Anomalous chain diffusion in unentangled model polymer nanocomposites. Soft Matter 2013;9:4336–48.
[149] Schneider GJ, Nusser K, Willner L, Falus P, Richter D. Dynamics of entangled chains in polymer nanocomposites. Macromolecules 2011;44:5857–60.
[150] Wei Y, Xu Y, Faraone A, Hore MJA. Local structure and relaxation dynamics in the brush of polymer-grafted silica nanoparticles. ACS Macro Lett 2018;7:699–704.
[151] Senses E, Tyagi M, Pasco M, Faraone A. Dynamics of architecturally engineered all-polymer nanocomposites. ACS Nano 2018;12:10807–16.
[152] Li Y, Kröger M, Liu WK. Nanoparticle effect on the dynamics of polymer chains and their entanglement network. Phys Rev Lett 2012;109, 118001/1-5.
[153] Smith GD, Bedrov D, Li L, Byutner O. A molecular dynamics simulation study of the viscoelastic properties of polymer nanocomposites. J Chem Phys 2002;117:9478–90.
[154] Dionne PJ, Ozisik R, Picu CR. Structure and dynamics of polyethylene nanocomposites. Macromolecules 2005;38:9351–8.
[155] Kalathi JT, Kumar SK, Rubinstein M, Grest GS. Rouse mode analysis of chain relaxation in polymer nanocomposites. Soft Matter 2015;11:4123–32.
[156] Picu RC, Rakshit A. Dynamics of free chains in polymer nanocomposites. J Chem Phys 2007;126, 144909/1-6.
[157] Nusser K, Neueder S, Schneider GJ, Meyer M, Pyckhout-Hintzen W, Willner L, et al. Conformations of silica-poly (ethylene-propylene) nanocomposites. Macromolecules 2010;43:9837–47.
[158] Yamamoto U, Schweizer KS. Theory of entanglements and tube confinement in rod-sphere nanocomposites. ACS Macro Lett 2013;2:955–9.
[159] Mangal R, Srivastava S, Narayanan S, Archer LA. Size-dependent particle dynamics in entangled polymer nanocomposites. Langmuir 2016;32:596–603.
[160] Li Y, Kröger M, Liu WK. Nanoparticle geometrical effect on structure, dynamics and anisotropic viscosity of polyethylene nanocomposites. Macromolecules 2012;45:2099–112.
[161] Karatrantos A, Composto RJ, Winey KI, Clarke N. Primitive path network, structure and dynamics of SWCNT/polymer nanocomposites. IOP Conf Ser Mater Sci Eng 2012;40:1–6.
[162] Karatrantos A, Clarke N, Composto RJ, Winey KI. Entanglements in polymer nanocomposites containing spherical nanoparticles. Soft Matter 2016;12:2567–74.
[163] Karatrantos A, Composto RJ, Winey KI, Kröger M, Clarke N. Entanglements and dynamics of polymer melts near a SWCNT. Macromolecules 2012;45:7274–81.
[164] Karatrantos A, Clarke N, Composto RJ, Winey KI. Topological entanglement length in polymer melts and nanocomposites by a DPD polymer model. Soft Matter 2013;9:3877–84.
[165] Riggleman RA, Toepperwein G, Papakonstantopoulos GJ, Barrat JL, De Pablo JJ. Entanglement network in nanoparticle reinforced polymers. J Chem Phys 2009;130, 244903/1-6.
[166] Karatrantos A, Clarke N, Composto RJ, Winey KI. Structure, entanglements and dynamics of polymer nanocomposites containing spherical nanoparticles. IOP Conf Ser Mater Sci Eng 2014;64:1–6.
[167] Klonos P, Kulyk K, Borysenko MV, Gun'ko VM, Kyritsis A, Pissis P. Effects of molecular weight below the entanglement threshold on interfacial Nanoparticles/Polymer dynamics. Macromolecules 2016;49: 9457–73.
[168] von Meerwall ED. Self-diffusion in polymer systems, measured with field-gradient spin echo NMR methods. Adv Polym Sci 1984;54: 1–29.
[169] Composto RJ, Walters RM, Genzer J. Application of ion scattering techniques to characterize polymer surfaces and interfaces. Mater Sci Eng R Rep 2002;38:107–80.
[170] Gam S, Meth JS, Zane SG, Chi C, Wood BA, Seitz ME, et al. Macromolecular diffusion in a crowded polymer nanocomposite. Macromolecules 2011;44:3494–501.
[171] Whitlow SJ, Wool RP. Diffusion of polymers at interfaces: a secondary ion mass spectroscopy study. Macromolecules 1991;24:5926–38.
[172] Segalman RA, Jacobson A, Kramer EJ, Lustig SR. Polymer diffusion in semicrystalline polymers using secondary ion mass spectroscopy. Macromolecules 2004;37:2613–7.
[173] Russell TP. X-ray and neutron reflectivity for the investigation of polymers. Mater Sci Eng R Rep 1990;5:171–271.
[174] Muthukumar M, Baumgaertner A. Effects of entropic barriers on polymer dynamics. Macromolecules 1989;22:1937–41.
[175] Muthukumar M, Baumgaertner A. Diffusion of a polymer chain in random media. Macromolecules 1989;22:1941–6.
[176] Huang XW, Peng Y, Huang JH, Luo MB. A study on the diffusivity of polymers in crowded environments with periodically distributed nanoparticles. Phys Chem Chem Phys 2017;19:29975–83.
[177] Yamamoto U, Schweizer KS. Theory of anisotropic diffusion of entangled and unentangled polymers in rod-sphere mixtures. ACS Macro Lett 2015;4:53–7.
[178] Meth JS, Zane SG, Chi C, Londono JD, Wood BA, Cotts P, et al. Development of filler structure in colloidal silica-polymer nanocomposites. Macromolecules 2011;44:8301–13.
[179] Maxwell JC. A treatise on electricity and magnetism. London: Oxford University Press; 1873, 444 pp.
[180] Lin CC, Gam S, Meth JS, Clarke N, Winey KI, Composto RJ. Do attractive polymer-nanoparticle interactions retard polymer diffusion in nanocomposites? Macromolecules 2013;46:4502–9.
[181] Gam S, Meth JS, Zane SG, Chi C, Wood BA, Winey KI, et al. Polymer diffusion in a polymer nanocomposite: effect of nanoparticle size and polydispersity. Soft Matter 2012;8:6512–20.
[182] Choi J, Hore MJA, Meth JS, Clarke N, Winey KI, Composto RJ. Universal scaling of polymer diffusion in nanocomposites. ACS Macro Lett 2013;2:485–90.
[183] Choi J, Hore MJA, Clarke N, Winey KI, Composto RJ. Nanoparticle brush architecture controls polymer diffusion in nanocomposites. Macromolecules 2014;47:2404–10.
[184] Meth JS, Gam S, Choi J, Lin CC, Composto RJ, Winey KI. Excluded volume model for the reduction of polymer diffusion into nanocomposites. J Phys Chem B 2013;117:15675–83.
[185] Choi J, Clarke N, Winey KI, Composto RJ. Polymer diffusion from attractive and athermal substrates. Macromolecules 2017;50:3038–42.
[186] Sauer BB, Zheng X, Rubinstein M, Rafailovich MH, Schwarz SA, Sokolov J, et al. Long-range effects on polymer diffusion induced by a bounding interface. Phys Rev Lett 2002;79:241–4.
[187] Choi KI, Kim TH, Yuan G, Satija SK, Koo J. Dynamics of entangled polymers confined between graphene oxide sheets as studied by neutron reflectivity. ACS Macro Lett 2017;6:819–23.
[188] Tung WS, Griffin PJ, Meth JS, Clarke N, Composto RJ, Winey KI. Temperature-dependent suppression of polymer diffusion in polymer nanocomposites. ACS Macro Lett 2016;5:735–9.
[189] Ozisik R, Zheng J, Dionne PJ, Picu CR, Von Meerwall ED. NMR relaxation and pulsed-gradient diffusion study of polyethylene nanocomposites. J Chem Phys 2005;123, 134901/1-8.
[190] Miller B, Imel AE, Holley W, Baskaran D, Mays JW, Dadmun MD. The role of nanoparticle rigidity on the diffusion of linear polystyrene in a polymer nanocomposite. Macromolecules 2015;48:8369–75.
[191] Martin HJ, White BT, Yuan G, Saito T, Dadmun MD. Relative size of the polymer and nanoparticle controls polymer diffusion in all-polymer nanocomposites. Macromolecules 2019;52:2843–52.
[192] Desai T, Keblinski P, Kumar SK. Molecular dynamics simulations of polymer transport in nanocomposites. J Chem Phys 2005;122, 134910/1-8.
[193] Sorichetti V, Hugouvieux V, Kob W. Structure and dynamics of a polymer-nanoparticle composite: effect of nanoparticle size and volume fraction. Macromolecules 2018;51:5375–91.
[194] Zhang H, Sun DD, Peng Y, Huang JH, Luo MB. Diffusivity and glass transition of polymer chains in polymer nanocomposites. Phys Chem Chem Phys 2019;21:23209–16.
[195] Karatrantos A, Composto RJ, Winey KI, Clarke N. Polymer and spherical nanoparticle diffusion in nanocomposites. J Chem Phys 2017;146, 203331/1-6.
[196] Mu M, Clarke N, Composto RJ, Winey KI. Polymer diffusion exhibits a minimuM. with increasing single-walled carbon nanotube concentration. Macromolecules 2009;42:7091–7.
[197] Mu M, Composto RJ, Clarke N, Winey KI. MinimuM. In diffusion coefficient with increasing MWCNT concentration requires tracer molecules to be larger than nanotubes. Macromolecules 2009;42:8365–9.
[198] Tung WS, Clarke N, Composto RJ, Winey KI. Temperature dependence of polymer diffusion in MWCNT/PS nanocomposites. Macromolecules 2013;46:2317–22.
[199] Lin CC, Ohno K, Clarke N, Winey KI, Composto RJ. Macromolecular diffusion through a polymer matrix with polymer-grafted chained nanoparticles. Macromolecules 2014;47:5357–64.
[200] Lin CC, Cargnello M, Murray CB, Clarke N, Winey KI, Riggleman RA, et al. Nanorod mobility influences polymer diffusion in polymer nanocomposites. ACS Macro Lett 2017;6:869–74.
[201] Choi J, Clarke N, Winey KI, Composto RJ. Fast polymer diffusion through nanocomposites with anisotropic particles. ACS Macro Lett 2014;3:886–91.
[202] Karatrantos A, Clarke N. A theoretical model for the prediction of diffusion in polymer/SWCNT nanocomposites. Soft Matter 2011;7:7334–41.
[203] Choi J, Cargnello M, Murray CB, Clarke N, Winey KI, Composto RJ. Fast nanorod diffusion through entangled polymer melts. ACS Macro Lett 2015;4:952–6.

[204] Lin EK, Kolb R, Satija SK, Wu WL. Reduced polymer mobility near the polymer/solid interface as measured by neutron reflectivity. Macromolecules 1999;32:3753–7.
[205] Zheng X, Sauer BB, Van Alsten JG, Schwarz SA, Rafailovich MH, Sokolov J, et al. Reptation dynamics of a polymer melt near an attractive solid interface. Phys Rev Lett 1995;74:407–10.
[206] Jimenez AM, Zhao D, Misquitta K, Jestin J, Kumar SK. Exchange lifetimes of the bound polymer layer on silica nanoparticles. ACS Macro Lett 2019;8:166–71.
[207] Bailey EJ, Griffin PJ, Composto RJ, Winey KI. Characterizing the areal density and desorption kinetics of physically adsorbed polymer in polymer nanocomposite melts. Macromolecules 2020;53(7):2744–53.
[208] Griffin PJ, Bocharova V, Middleton LR, Composto RJ, Clarke N, Schweizer KS, et al. Influence of the bound polymer layer on nanoparticle diffusion in polymer melts. ACS Macro Lett 2016;5:1141–5.
[209] Jouault N, Crawford MK, Chi C, Smalley RJ, Wood B, Jestin J, et al. Polymer chain behavior in polymer nanocomposites with attractive interactions. ACS Macro Lett 2016;5:523–7.
[210] Jouault N, Moll JF, Meng D, Windsor K, Ramcharan S, Kearney C, et al. Bound polymer layer in nanocomposites. ACS Macro Lett 2013;2:371–4.
[211] Cai LH, Panyukov S, Rubinstein M. Mobility of nonsticky nanoparticles in polymer liquids. Macromolecules 2011;44:7853–63.
[212] Cai LH, Panyukov S, Rubinstein M. Hopping diffusion of nanoparticles in polymer matrices. Macromolecules 2015;48:847–62.
[213] Dell ZE, Schweizer KS. Theory of localization and activated hopping of nanoparticles in cross- linked networks and entangled polymer melts. Macromolecules 2014;47:405–14.
[214] Yamamoto U, Carrillo JMY, Bocharova V, Sokolov AP, Sumpter BG, Schweizer KS. Theory and simulation of attractive nanoparticle transport in polymer melts. Macromolecules 2018;51:2258–67.
[215] Yamamoto U, Schweizer KS. Theory of nanoparticle diffusion in unentangled and entangled polymer melts. J Chem Phys 2011;135, 224902/1-16.
[216] Yamamoto U, Schweizer KS. Microscopic theory of the long-time diffusivity and intermediate- time anomalous transport of a nanoparticle in polymer melts. Macromolecules 2015;48:152–63.
[217] Yamamoto U, Schweizer KS. Spatially dependent relative diffusion of nanoparticles in polymer melts. J Chem Phys 2013;139, 064907/1-10.
[218] Ganesan V, Pryamitsyn V, Surve M, Narayanan B. Noncontinuum effects in nanoparticle dynamics in polymers. J Chem Phys 2006;124, 221102/1-4.
[219] Egorov SA. Anomalous nanoparticle diffusion in polymer solutions and melts: a mode-coupling theory study. J Chem Phys 2011;134, 084903/1-6.
[220] Wöll D. Fluorescence correlation spectroscopy in polymer science. RSC Adv 2014;4:2447–65.
[221] Grabowski CA, Mukhopadhyay A. Size effect of nanoparticle diffusion in a polymer melt. Macromolecules 2014;47:7238–42.
[222] Nath P, Mangal R, Kohle F, Choudhury S, Narayanan S, Wiesner U, et al. Dynamics of nanoparticles in entangled polymer solutions. Langmuir 2018;34:241–9.
[223] Parrish E, Seeger SC, Composto RJ. Temperature-dependent nanoparticle dynamics in poly(N- isopropylacrylamide) gels. Macromolecules 2018;51:3597–607.
[224] Manzo C, Garcia-Parajo MF. A review of progress in single particle tracking: from methods to biophysical insights. Rep Prog Phys 2015;78, 124601/1-29.
[225] Park J, Bailey EJ, Composto RJ, Winey KI. Single particle tracking of non-sticky and sticky nanoparticles in polymer melts. Macromolecules 2020, http://dx.doi.org/10.1021/acs.macromol.0c00457.
[226] Xue C, Zheng X, Chen K, Tian Y, Hu G. Probing non-gaussianity in confined diffusion of nanoparticles. J Phys Chem Lett 2016;7:514–9.
[227] Lungova M, Krutyeva M, Pyckhout-Hintzen W, Wischnewski A, Monkenbusch M, Allgaier J, et al. Nanoscale motion of Soft nanoparticles in unentangled and entangled polymer matrices. Phys Rev Lett 2016;117, 147803/1-5.
[228] Kalathi JT, Yamamoto U, Schweizer KS, Grest GS, Kumar SK. Nanoparticle diffusion in polymer nanocomposites. Phys Rev Lett 2014;112, 108301/1-5.
[229] Liu J, Cao D, Zhang L. Molecular dynamics study on nanoparticle diffusion in polymer melts: a test of the Stokes-Einstein law. J Phys Chem C 2008;112:6653–61.
[230] Ge T, Kalathi JT, Halverson JD, Grest GS, Rubinstein M. Nanoparticle motion in entangled melts of linear and nonconcatenated ring polymers. Macromolecules 2017;50:1749–54.
[231] Medidhi KR, Padmanabhan V. Diffusion of polymer-grafted nanoparticles in a homopolymer matrix. J Chem Phys 2019;150, 044905/1-7.
[232] Chen T, Qian HJ, Lu ZY. Diffusion dynamics of nanoparticle and its coupling with polymers in polymer nanocomposites. Chem Phys Lett 2017;687:96–100.
[233] Karatrantos A, Composto RJ, Winey KI, Clarke N. Nanorod diffusion in polymer nanocomposites by molecular dynamics simulations. Macromolecules 2019;52:2513–20.
[234] Tuteja A, Mackay ME, Narayanan S, Asokan S, Wong MS. Breakdown of the continuum Stokes- Einstein relation for nanoparticle diffusion. Nano Lett 2007;7:1276–81.
[235] Grabowski CA, Adhikary B, Mukhopadhyay A. Dynamics of gold nanoparticles in a polymer melt. Appl Phys Lett 2009;94:1–4.
[236] Lin CC, Griffin PJ, Chao H, Hore MJA, Ohno K, Clarke N, et al. Grafted polymer chains suppress nanoparticle diffusion in athermal polymer melts. J Chem Phys 2017;146, 203332/1-8.
[237] Kim MJ, Cho HW, Kim MJ, Kim H, Sung BJ. Translational and rotational diffusion of a single nanorod in unentangled polymer melts. Phys Rev E 2015;92, 042601/1-8.
[238] Alam S, Mukhopadhyay A. Translational and rotational diffusions of nanorods within semidilute and entangled polymer solutions. Macromolecules 2014;47:6919–24.
[239] Riseman J, Kirkwood JG. The intrinsic viscosity, translational and rotatory diffusion constants of rod-like macromolecules in solution. J Chem Phys 1950;18:512–6.
[240] Tsay JM, Doose S, Weiss S. Rotational and translational diffusion of peptide-coated CdSe/CdS/ZnS nanorods studied by fluorescence correlation spectroscopy. J Am Chem Soc 2006;128:1639–47.
[241] Poling-Skutvik R, Mongcopa KIS, Faraone A, Narayanan S, Conrad JC, Krishnamoorti R. Structure and dynamics of interacting nanoparticles in semidilute polymer solutions. Macromolecules 2016;49: 6568–77.
[242] Poling-Skutvik R, Krishnamoorti R, Conrad JC. Size-dependent dynamics of nanoparticles in unentangled polyelectrolyte solutions. ACS Macro Lett 2015;4:1169–73.
[243] Poling-Skutvik R, Slim AH, Narayanan S, Conrad JC, Krishnamoorti R. Soft interactions modify the diffusive dynamics of polymer-grafted nanoparticles in solutions of free polymer. ACS Macro Lett 2019;8: 917–22.
[244] Senanayake KK, Fakhrabadi EA, Liberatore MW, Mukhopadhyay A. Diffusion of nanoparticles in entangled poly(vinyl alcohol) solutions and gels. Macromolecules 2019;52:787–95.
[245] Senanayake KK, Mukhopadhyay A. Nanoparticle diffusion within dilute and semidilute xanthan solutions. Langmuir 2019;35:7978–84.
[246] Carroll B, Bocharova V, Carrillo JMY, Kisliuk A, Cheng S, Yamamoto U, et al. Diffusion of sticky nanoparticles in a polymer melt: crossover from suppressed to enhanced transport. Macromolecules 2018;51: 2268–75.
[247] Ren KX, Jia XM, Jiao GS, Chen T, Qian HJ, Lu ZY. Interfacial properties and hopping diffusion of small nanoparticle in polymer/nanoparticle composite with attractive interaction on side group. Polymers 2018; 10, 598/1-18.
[248] Volgin IV, Larin SV, Abad E, Lyulin SV. Molecular dynamics simulations of fullerene diffusion in polymer melts. Macromolecules 2017;50:2207–18.
[249] Volgin IV, Larin SV, Lyulin AV, Lyulin SV. Coarse-grained molecular-dynamics simulations of nanoparticle diffusion in polymer nanocomposites. Polymer 2018;145:80–7.
[250] Cao XZ, Merlitz H, Wu CX. Tuning adsorption duration to control the diffusion of a nanoparticle in adsorbing polymers. J Phys Chem Lett 2017;8:2629–33.
[251] Karatrantos A, Koutsawa Y, Dubois P, Clarke N, Kröger M. Miscibility and nanoparticle diffusion in ionic nanocomposites. Polymers 2018;10, 1010/1-16.
[252] Senses E, Tyagi M, Natarajan B, Narayanan S, Faraone A. Chain dynamics and nanoparticle motion in attractive polymer nanocomposites subjected to large deformations. Soft Matter 2017;13:7922–9.
[253] Jang WS, Koo P, Bryson K, Narayanan S, Sandy A, Russell TP, et al. Dynamics of cadmium sulfide nanoparticles within polystyrene melts. Macromolecules 2014;47:6483–90.
[254] Srivastava S, Archer LA, Narayanan S. Structure and transport anomalies in soft colloids. Phys Rev Lett 2013;110, 148302/1-5.
[255] Narayanan RA, Thiyagarajan P, Lewis S, Bansal A, Schadler LS, Lurio LB. Dynamics and internal stress at the nanoscale related to unique thermomechanical behavior in polymer nanocomposites. Phys Rev Lett 2006;97, 075505/1-4.
[256] Kim D, Srivastava S, Narayanan S, Archer LA. Polymer nanocomposites: polymer and particle dynamics. Soft Matter 2012;8:10813–8.
[257] Yang S, Liu S, Narayanan S, Zhang C, Akcora P. Chemical heterogeneity in interfacial layers of polymer nanocomposites. Soft Matter 2018;14:4784–91.
[258] Srivastava S, Kandar AK, Basu JK, Mukhopadhyay MK, Lurio LB, Narayanan S, et al. Complex dynamics in polymer nanocomposites. Phys Rev E 2009;79, 021408/1-7.
[259] Hoshino T, Murakami D, Tanaka Y, Takata M, Jinnai H, Takahara A. Dynamical crossover between hyperdiffusion and subdiffusion of polymer-grafted nanoparticles in a polymer matrix. Phys Rev E 2013;88, 032602/1-7.
[260] Ranka M, Varkey N, Ramakrishnan S, Zukoski CF. Impact of small changes in particle surface chemistry for unentangled polymer nanocomposites. Soft Matter 2015;11:1634–45.
[261] Senses E, Narayanan S, Mao Y, Faraone A. Nanoscale particle motion in attractive polymer nanocomposites. Phys Rev Lett 2017;119, 237801/1-5.
[262] Srivastava S, Agarwal P, Mangal R, Koch DL, Narayanan S, Archer LA. Hyperdiffusive dynamics in newtonian nanoparticle fluids. ACS Macro Lett 2015;4:1149–53.
[263] Liu S, Senses E, Jiao Y, Narayanan S, Akcora P. Structure and entanglement factors on dynamics of polymer-grafted nanoparticles. ACS Macro Lett 2016;5:569–73.
[264] Song JJ, Bhattacharya R, Kim H, Chang J, Tang TY, Guo H, et al. One-dimensional anomalous diffusion of gold nanoparticles in a polymer melt. Phys Rev Lett 2019;122, 107802/1-6.
[265] Guo H, Bourret G, Corbierre MK, Rucareanu S, Lennox RB, Laaziri K, et al. Nanoparticle motion within glassy polymer melts. Phys Rev Lett 2009;102, 075702/1-4.

[266] Senses E, Narayanan S, Faraone A. Nanoscale particle motion reveals polymer mobility gradient in nanocomposites. ACS Macro Lett 2019;8:558–62.
[267] Kandar AK, Srivastava S, Basu JK, Mukhopadhyay MK, Seifert S, Narayanan S. Unusual dynamical arrest in polymer grafted nanoparticles. J Chem Phys 2009;130:1–6.
[268] Dierker SB, Pindak R, Fleming RM, Robinson IK, Berman L. X-Ray photon correlation spectroscopy study of Brownian motion of gold colloids in glycerol. Phys Rev Lett 1995;75:449–52.
[269] Leheny RL. XPCS: nanoscale motion and rheology. Curr Opin Colloid Interface Sci 2012;17:3–12.
[270] Genix AC, Oberdisse J. Structure and dynamics of polymer nanocomposites studied by X-ray and neutron scattering techniques. Curr Opin Colloid Interface Sci 2015;20:293–303.
[271] Bras W, Stanley H. Unexpected effects in non crystalline materials exposed to X-ray radiation. J Non Cryst Solids 2016;451:153–60.
[272] Genix AC, Bocharova V, Carroll B, Lehmann M, Saito T, Krueger S, et al. Understanding the static interfacial polymer layer by exploring the dispersion states of nanocomposites. ACS Appl Mater Interfaces 2019;11:17863–72.
[273] Gin P, Jiang N, Liang C, Taniguchi T, Akgun B, Satija SK, et al. Revealed architectures of adsorbed polymer chains at solid-polymer melt interfaces. Phys Rev Lett 2012;109, 265501/1-5.
[274] Jouault N, Zhao D, Kumar SK. Role of casting solvent on nanoparticle dispersion in polymer nanocomposites. Macromolecules 2014;47:5246–55.
[275] Lepcio P, Ondreas F, Zarybnicka K, Zboncak M, Caha O, Jancar J. Bulk polymer nanocomposites with preparation protocol governed nanostructure: the origin and properties of aggregates and polymer bound clusters. Soft Matter 2018;14:2094–103.